

# Toward end-to-end quantum simulation for protein dynamics

Zhenning Liu<sup>1,2</sup>, Xiantao Li<sup>3</sup>, Chunhao Wang<sup>4</sup>, Jin-Peng Liu<sup>5,6</sup>

<sup>1</sup> Joint Center for Quantum Information and Computer Science, University of Maryland

<sup>2</sup> Department of Computer Science, University of Maryland

<sup>3</sup> Department of Mathematics, Pennsylvania State University

<sup>4</sup> Department of Computer Science and Engineering, Pennsylvania State University

<sup>5</sup> Yau Mathematical Sciences Center, Tsinghua University

<sup>6</sup> Beijing Institute of Mathematical Sciences and Applications

## Abstract

Modeling and simulating the protein folding process overall remains a grand challenge in computational biology. We systematically investigate end-to-end quantum algorithms for simulating various protein dynamics with effects, such as mechanical forces or stochastic noises. We offer efficient quantum simulation algorithms to produce quantum encoding of the final states, history states, or density matrices of inhomogeneous or stochastic harmonic oscillator models. For the read-in setting, we design (i) efficient quantum algorithms for initial state preparation, utilizing counter-based random number generator and rejection sampling, and (ii) depth-efficient approaches for molecular structure loading. Both are particularly important in handling large protein molecules. For the read-out setting, our algorithms estimate various classical observables, such as energy, low vibration modes, density of states, correlation of displacement, and optimal control of molecular dynamics. We also show classical numerical experiments focused on estimating the density of states and applying the optimal control to facilitate conformation changes to verify our arguments on potential quantum speedups. Overall, our study demonstrates that the quantum simulation of protein dynamics can be a solid end-to-end application in the era of early or fully fault-tolerant quantum computing.

## 1 Introduction

The precise functions of biological systems frequently hinge on the ability of proteins to undergo conformational transitions. These structural changes encompass a broad range of movements — from minor adjustments of individual side-chains and loops to extensive shifts involving large domains. To thoroughly understand and predict these dynamic processes, it is crucial to simulate the motions of protein atoms over biologically relevant timescales, enabling the identification of key atomic properties that dictate protein function, e.g., in target-based drug designing, elucidating protein-related disease mechanisms, and innovating novel enzymes. However, current molecular dynamics simulations face significant challenges in this domain. While they are effective for exploring small-scale transitions, the computational demands of these methods become prohibitive when

studying more extensive molecular motions. This limitation stems from the inadequate sampling of conformational space within the typical simulation durations of just tens of nanoseconds, which are insufficient to capture large-scale dynamics. Moreover, the complexity of protein structures, characterized by numerous local minima due to their large number of atoms, further complicates the simulation process. Thus, modeling and simulating the protein folding process overall remains a grand challenge in computational biology. While recent advancements in AI-based methods such as AlphaFold3 [63], their precision in determining the structure of the protein with low sequence similarity is still limited.

Recent advances in quantum computing offer a new perspective on the study of protein structure problems. Generally, prior work mapped the coarse-grained protein folding problems onto unconstrained or constrained optimization problems, for which they explored near-term algorithms such as quantum annealing algorithms, Variational Quantum Eigensolver (VQE), and Quantum Approximated Optimization Algorithm (QAOA) to obtain heuristic solutions [13, 47, 93, 59, 80, 23, 42]. While these algorithms are feasible for current Noisy Intermediate-Scale Quantum (NISQ) devices, a provable quantum speedup has yet to be established.

Meanwhile, quantum algorithms have been extensively proposed to simulate quantum dynamics as well as general linear differential equations on early or fully fault-tolerant quantum devices. This approach provides the quantum states that encode the solution of high-dimensional dynamical systems, only requiring complexity polynomial logarithmic in terms of the dimension, which may offer potential exponential speedup over classical algorithms. A large variety of quantum algorithms have been developed for Hamiltonian simulations [84, 17, 19, 18, 86, 85], solving systems of linear equations [56, 2, 30, 4, 77] and differential equations [16, 20, 32, 33, 82, 5, 6], as well as open quantum systems [69, 31, 34, 73, 74, 27, 38, 90]. A critical remaining challenge is developing preparation protocols and measurement tools in order to maintain the end-to-end quantum advantage. Recent work [11] investigates quantum simulation of high-dimensional coupled oscillator systems and raises potential applications in classical dynamical systems. However, for different practical models of protein dynamics, which can involve non-Hermitian systems, stochastic forces, and various target properties as outputs, the corresponding efficient quantum algorithms are still less understood.

In this work, we systematically investigate end-to-end quantum algorithms for simulating various protein dynamics with effects, such as mechanical forces or stochastic noises. Such problems can be formulated as harmonic approximation systems or general non-Hermitian dynamics. We offer efficient quantum simulation algorithms by leveraging Hamiltonian Simulation (HS), quantum linear Ordinary Differential Equation (ODE) solvers, Linear Combination of Hamiltonian Simulation (LCHS), and open quantum system simulation to produce quantum encoding of the final states, history states, or density matrices.

For the read-in setting, we design efficient algorithms for both initial state preparation (ISP) and matrix connectivity loading (MCL) for protein dynamics simulation, which is particularly important in handling large protein molecules. We briefly outline both results in the following paragraphs. We use  $N$  to denote the number of oscillators in the model.

In many popular coupled-oscillator models of protein dynamics (such as the *Gaussian network*

model), initial positions and velocities of oscillators are sampled from Gaussian distributions. If these initial configurations are amplitude encoded as quantum states of  $\mathcal{O}(\log N)$  qubits, then these states are *Gaussian random amplitude states*, pure states with all coefficients in the computational basis sampled from Gaussian distributions. In this paper, we identify two categories of initial states, corresponding to two types of protein dynamics simulation tasks: *ensemble simulation* and *single-state simulation*. The former’s purpose is estimating average quantities over all possible initial configurations, while the latter aims at studying the dynamics of one or few specific physically meaningful random initial configurations. For ensemble simulation, we prove that the convex combination of all Gaussian random amplitude states weighted by their probability densities is simply the maximally mixed state,  $\rho_G \propto \sum_i |i\rangle \langle i|$ , an easy-to-prepare state. For single-state simulation, we develop a novel quantum algorithm with  $\text{polylog}(N)$  gate complexity to prepare Gaussian *pseudo-random* states, achieving an exponential saving in qubit number over previous results in preparing Gaussian (true-)random states [24]. (Note that pseudo-random numbers suffice for performing simulations, since this is used in classical simulation algorithms.) Our algorithm contains a series of binary data loaders, whose rotation angles follow the distribution shown in in Ref. [24] and are generated by a *quantized rejection sampling* approach. The (pseudo-)randomness of the state is provided by quantized *counter-based pseudo-random number generators* (CBRNG), quantization of the standard parallel random number generator. This allows us to reproduce or modify each specific pseudo-randomly sampled state repeatedly. We summarize our results in initial state preparation in Table 1.

<b>Problem</b>	<b>Results</b>	<b>Algorithm</b>	<b>Gate complexity</b>
ISP for ensemble simulation <b>Problem 1</b>	<b>Theorem 4.3</b>	Parallel Hadamard gates	$\mathcal{O}(\log N)$
ISP for single-state simulation <b>Problem 2</b>	<b>Theorem 4.4</b>	Quantized rejection sampling	$\text{polylog}(N)$

Table 1: Summary of initial state preparation (ISP) results.

We recognize that loading the matrix  $K$  describing the connectivity of the coupled oscillator system into the quantum algorithm is particularly difficult in simulating protein dynamics. This is because all information in  $K$  is provided by, e.g., laboratory observations or computer simulations, and cannot be compressed to  $\mathcal{O}(\log N)$  classical bits. Therefore, we focus on designing low-depth data loading approaches for  $K$ . We present the construction of the standard sparse oracle using quantum read-only memory (QROM) which can be implemented in  $\text{polylog}(N)$  depth. Besides the brute-force sparse access, we also design a flexible binary tree data structure via QROM. This can be used to efficiently modify the protein structure, including changing the masses or positions of oscillators and adding or removing atoms or residues, by modifying  $\mathcal{O}(d \text{polylog}(N))$  entries of the QROM, rather than  $\mathcal{O}(d^2)$  in the brute-force case. We summarize our results in matrix connectivity loading in Table 2.

Problem	Results	Gate complexity	Circuit depth	Modification
Low-depth MCL <a href="#">Problem 3</a>	<a href="#">Theorem 5.1</a>	$\mathcal{O}(N \cdot \text{polylog } N)$	$\text{polylog}(N)$	$\mathcal{O}(d^2)$
MCL with efficient modification <a href="#">Problem 4</a>	<a href="#">Theorem 5.2</a>	$\mathcal{O}(N \cdot \text{polylog } N)$	$\text{polylog}(N)$	$\mathcal{O}(d \cdot \text{polylog } N)$

Table 2: Summary of matrix connectivity loading (MCL) results.

For the read-out setting, we consider the quantum evolution (QE) model and the block-encoding (BE) model. Our algorithms estimate various classical observables, such as energy, low vibration modes, density of states, correlation of displacement, and optimal control of molecular dynamics. We also design classical numerical experiments, focused on estimating the density of states and applying the optimal control to facilitate conformation changes. These tests are conducted on classical devices to demonstrate the feasibility of the algorithms. Our study shows that quantum algorithms for simulating protein dynamics and computing protein properties can be a solid end-to-end application in the era of early or fully fault-tolerant quantum computing.

Problem	Algorithm	Results	Complexity
Harmonic oscillator <a href="#">Problem 5</a>	Hamiltonian simulation	<a href="#">Theorem 6.1</a>	$\mathcal{O}(\sqrt{\kappa_A}T + \log(1/\epsilon))$
Inhomogeneous harmonic oscillator <a href="#">Problem 6</a>	LCHS	<a href="#">Theorem 6.2</a>	$\mathcal{O}(\sqrt{\kappa_A}T \log^{1+1/\beta}(1/\epsilon))$
History-state model <a href="#">Problem 7</a>	Quantum linear ODE solver	<a href="#">Theorem 6.3</a>	$\mathcal{O}(\sqrt{\kappa_A}T \text{polylog}(1/\epsilon))$
Langevin dynamics <a href="#">Problem 8</a>	Open quantum system simulation	<a href="#">Theorem 6.4</a>	$\mathcal{O}(\sqrt{\kappa_A}T + \log(1/\epsilon))$

Table 3: Summary of quantum simulation algorithms for the protein dynamics. Here  $n$  is the number of protein molecules,  $\kappa$  is the norm of  $A = (\sqrt{M})^{-1}K(\sqrt{M})^{-1}$ ,  $T$  is the evolution time, and  $\beta \in (0, 1)$ . LCHS: linear combination of Hamiltonian simulation.

Problem	Algorithm	Results	Complexity	Model
Kinetic and potential energy	HS and AA	<a href="#">Theorem 7.1</a> , <a href="#">Theorem 7.2</a>	$\mathcal{O}(1/\epsilon)$	QE
Low vibration modes	HS and AA	<a href="#">Theorem 7.3</a> , <a href="#">Theorem 7.4</a>	$\mathcal{O}(1/(\gamma\epsilon))$	QE
Density of States, Chebyshev moments	QSVT and AA	<a href="#">Theorem 7.6</a>	$\mathcal{O}(\alpha/\epsilon^2)$ , $\mathcal{O}(\alpha k/\epsilon)$	BE
Correlation, root mean square displacement	QSVT and AA	<a href="#">Theorem 7.8</a>	$\mathcal{O}(\alpha/\epsilon)$	BE
Molecular dynamical control	HS and AA	<a href="#">Theorem 7.9</a>	$\mathcal{O}(\beta/\epsilon)$	QE

Table 4: Summary of end-to-end quantum applications for the protein dynamics. Here  $\epsilon$  is the error tolerance,  $\alpha, \beta$  are the block-encoding factors of Hamiltonian  $H$  and observable  $O$ ,  $\gamma$  is the overlap between initial and ground states,  $k$  is the degree of the Chebyshev moment. HS: Hamiltonian simulation. AA: amplitude amplification. QSVT: quantum singular value transformation. QE: quantum evolution model. BE: block-encoding model.

The rest of the paper is organized as follows. [Section 2](#) introduces notations, access models, and

QROM/QRAM. [Section 3](#) presents the normal mode analysis (NMA) that models the vibrational modes of protein dynamics. [Section 4](#) proposes the initial state preparation protocols. [Section 5](#) proposes the matrix loading protocols. [Section 6](#) presents quantum algorithms for simulating the protein dynamics. [Section 7](#) discusses several properties of protein as the read-outs. [Section 8](#) presents numerical experiments to verify our arguments. Finally, we conclude and discuss open questions in [Section 9](#).

## 2 Preliminaries

### 2.1 Notations

Let  $u = (u_0, u_1, \dots, u_{N-1})^T$  be an  $N$ -dimensional (possibly unnormalized) column vector. We use  $u^*$  to denote its conjugate transpose,  $\|u\|$  to denote its vector 2-norm, and  $\|u\|_1$  to denote its vector 1-norm. The notation  $|u\rangle$  represents a (pure) quantum state that is the normalized vector under 2-norm

$$|u\rangle = u/\|u\|. \quad (2.1)$$

For quantum states, we follow the standard bra-ket notation where  $\langle u|$  denotes the conjugate transpose of  $|u\rangle$  and  $\langle u|v\rangle$  denotes the inner product between  $|u\rangle$  and  $|v\rangle$ .

Let  $A$  be an  $N$ -by- $N$  matrix. We use  $A^\dagger$  to denote its conjugate transpose, *i.e.*, the adjoint operator of  $A$ . The norm  $\|A\|$  without subscript represents the spectral norm, *i.e.*, the matrix 2-norm

$$\|A\| = \sup_{u \neq 0} \|Au\|/\|u\|. \quad (2.2)$$

The norm  $\|A\|_1$  with subscript 1 is the Schatten 1-norm

$$\|A\|_1 = \text{Tr} \left( \sqrt{A^\dagger A} \right). \quad (2.3)$$

The trace distance between two matrices  $A$  and  $B$  is defined to be  $\frac{1}{2}\|A-B\|_1$ , and the trace distance between two pure states  $|u\rangle$  and  $|v\rangle$  is the trace distance between the corresponding density matrices  $|u\rangle\langle u|$  and  $|v\rangle\langle v|$ .

Let two functions  $f, g: \mathbb{R}_{>0} \rightarrow \mathbb{R}_{>0}$  represent some complexity scalings. We write  $f = \mathcal{O}(g)$  if there exists a constant  $C > 0$ , independent of the arguments of  $f$  and  $g$ , such that  $f(x) \leq Cg(x)$  for all sufficiently large  $x$ .  $f = \Omega(g)$  if  $g = \mathcal{O}(f)$ .  $f = \Theta(g)$  if  $f = \mathcal{O}(g)$  and  $f = \Omega(g)$ .  $f = \tilde{\mathcal{O}}(g)$  if  $f = \mathcal{O}(g \text{ poly } \log(g))$ .

### 2.2 Access models and block-encoding

We define the matrix and state preparation oracle access that is commonly used in quantum algorithms.

**Definition 2.1** (Matrix access). Suppose  $A$  can be accessed through the following oracle

$$O_r|i, k\rangle = |i, r_{ik}\rangle, \quad (2.4)$$

$$O_c|i, k\rangle = |i, c_{ik}\rangle, \quad (2.5)$$

$$O_a|i, j\rangle|0_b\rangle = |i, j\rangle|A(i, j)\rangle, \quad (2.6)$$

where  $r_{ij}$  (resp.  $c_{ij}$ ) are the  $j$ -th nonzero entry in the  $i$ -th row (resp. column), and  $A(i, j)$  is the binary representation of the  $(i, j)$  matrix entry of  $A$ .

**Definition 2.2** (State preparation). Let  $y$  be a  $2^n$ -dimensional vector and  $\|y\|_1 \leq \beta$ . Then a unitary  $U_I$  is a  $(\beta, n, 0)$ -state-preparation oracle, if  $U_I|0\rangle = \frac{1}{\beta} \sum_{j=0}^{2^n-1} y_j |j\rangle$ .

Block-encoding is a powerful technique to represent arbitrary matrices with unitary matrices. For a possibly non-unitary matrix  $A$  and a parameter  $\alpha \geq \|A\|$ , the intuitive idea of block-encoding is to construct a unitary  $U$  with higher dimension such that  $A$  appears in its upper-left block,

$$U = \begin{pmatrix} A/\alpha & * \\ * & * \end{pmatrix}. \quad (2.7)$$

More results about the block-encoding refer to [50].

**Definition 2.3** (Block-encoding). Suppose  $A$  is a  $2^n$ -dimensional matrix such that  $\|A\| \leq \alpha$ . Then a  $2^{n+a}$ -dimensional unitary matrix  $U$  is an  $(\alpha, a, \epsilon)$ -block-encoding of  $A$ , if

$$\|A - \alpha(\langle 0|_a \otimes I)U(|0\rangle_a \otimes I)\| \leq \epsilon. \quad (2.8)$$

Block-encoding allows us to encode a general matrix on quantum computers and then perform matrix operations, including summation, multiplication, inverse, and polynomial transformation. Here we mostly follow [50] again and briefly summarize several properties that will be used in our work.

**Definition 2.4** (State preparation pair). Let  $y$  be a  $2^n$ -dimensional vector and  $\|y\|_1 \leq \beta$ . Then a pair of unitaries  $(U_{IL}, U_{IR})$  is a  $(\beta, n, 0)$ -state-preparation-pair, if  $U_{IL}|0\rangle = \sum_{j=0}^{2^n-1} c_j |j\rangle$ ,  $U_{IR}|0\rangle = \sum_{j=0}^{2^n-1} d_j |j\rangle$  and  $\beta c_j^* d_j = y_j$  for any  $0 \leq j \leq 2^n - 1$ .

**Lemma 2.5** (Linear combination of block-encodings [50, Lemma 52]). Let  $A = \sum_{j=0}^{2^k-1} y_j A_j$  be a  $2^n$ -dimensional matrix. Suppose that  $(U_{IL}, U_{IR})$  is a  $(\beta, k, 0)$ -state-preparation-pair of  $y$ , and  $W = \sum_{j=0}^{2^k-1} |j\rangle \langle j| \otimes U_j$  is a  $2^{n+a+k}$ -dimensional unitary matrix such that  $U_j$  is an  $(\alpha, a, \epsilon)$ -block-encoding of  $A_j$ . Then  $(U_{IL}^\dagger \otimes I_a \otimes I_n)W(U_{IR} \otimes I_a \otimes I_n)$  is an  $(\alpha\beta, a+k, \alpha\beta\epsilon)$ -block-encoding of  $A$ , with a single use of  $W, U_{IL}^\dagger$  and  $U_{IR}$ .

**Lemma 2.6** (Multiplication of block-encodings [50, Lemma 53]). Let  $A, B$  be  $2^n$ -dimensional matrices,  $U_A$  be an  $(\alpha, a, \delta)$ -block-encoding of  $A$ , and  $U_B$  be a  $(\beta, b, \epsilon)$ -block-encoding of  $B$ . Then  $(I_b \otimes U_A)(I_a \otimes U_B)$  is an  $(\alpha\beta, a+b, \alpha\epsilon + \beta\delta)$ -block-encoding of  $AB$ , with a single use of  $U_A$  and  $U_B$ .

**Lemma 2.7** (Inverse of a block-encoding [99, Appendix B]). Suppose  $A$  is a  $2^n$ -dimensional invertible Hermitian matrix such that all the eigenvalues are within  $[-1, -\delta] \cup [\delta, 1]$ , and  $U_A$  is a  $(1, a, 0)$ -block-encoding of  $A$ . Then a  $(4/(3\delta), a+1, \epsilon)$ -block-encoding of  $A^{-1}$  can be constructed, using  $\mathcal{O}((1/\delta) \log(1/(\delta\epsilon)))$  queries to  $U_A$  and its inverse.

**Lemma 2.8** (Polynomial of a block-encoding [50, Theorem 56]). *Let  $A$  be a  $2^n$ -dimensional Hermitian matrix, and  $U_A$  is an  $(\alpha, a, \epsilon)$ -block-encoding of  $A$ . If  $P(x)$  is a degree- $d$  real polynomial such that  $|P(x)| \leq 1/2$  for all  $x \in [-1, 1]$ , then a  $(1, a + 2, 4d\sqrt{\epsilon/\alpha})$ -block-encoding of  $P(A/\alpha)$  can be constructed using  $d$  applications of  $U_A$  and  $U_A^\dagger$ , a single application of controlled  $U$  and  $\mathcal{O}((a+1)d)$  additional one- and two-qubit gates.*

We use the following technical tool to estimate the expectation of block-encoded observables.

**Lemma 2.9** ([92]). *Let  $O$  be an observable whose block-encoding has normalizing constant  $\alpha$  and construction cost  $Q$ . If a purification of a state  $\rho$  can be prepared with cost  $R$ , then for every  $\epsilon, \delta > 0$ , there exists a quantum algorithm that produces an estimate  $\xi$  of  $\text{Tr}(\rho O)$  such that*

$$|\xi - \text{Tr}(\rho O)| \leq \epsilon$$

*with probability at least  $1 - \delta$ . This algorithm has gate complexity  $\mathcal{O}((R + Q)_\epsilon^\alpha \log(1/\delta))$ .*

### 2.3 QROM and QRAM

In this paper, we use Quantum Read-Only Memory (QROM) [12, 89] (also known as Quantum Random-Access Classical Memory, QRACM, as a read-only version of QRAM) as a time-efficient method of loading classical data into the quantum algorithm. QROMs can coherently give the data corresponding to an address according to a classical dictionary. For instance, if a dictionary is given such that for every index  $i \in \{1, 2, \dots, N\}$  the data is an arbitrary  $v_i \in \{1, 2, \dots, M\}$ , then a QROM of this dictionary implements the following unitary:

$$\sum_i \alpha_i |i\rangle |0\rangle \mapsto \sum_i \alpha_i |i\rangle |v_i\rangle. \quad (2.9)$$

Many proposals for QROM or QRAM are available in the literature and they are either *passive* or *active* [62]. Passive QROMs can realize the data loading operation just like a single quantum gate without sophisticated error correction, such as [51], but are considered impractical because an exponentially low error rate is required [62]. Instead, we focus on active QROM/QRAMs that can be constructed explicitly by quantum circuits of  $\tilde{O}(N)$  gates but in  $\mathcal{O}(\log N)$  depth, when the amount of data stored is  $\mathcal{O}(N)$ . We notice that we aim at achieving exponential speedup in terms of  $N$ , but QROM's gate complexity scales linearly in  $N$ . We claim that this is an unavoidable cost, as shown in Theorem 2.10 also proved in [62]. We instead focus on achieving an exponential speedup in time complexity in this paper.

**Theorem 2.10** (Gate complexity lower bound of data loading). *Suppose there is a unitary  $U$  such that for all  $\sum_{i=1}^N \alpha_i |i\rangle$  with  $\sum_{i=1}^N |\alpha_i|^2 = 1$ , and for any ancilla register in state  $|R\rangle$ ,*

$$U \left[ |R\rangle \otimes \sum_{i=1}^N \alpha_i |i\rangle |0\rangle \right] = |R\rangle \otimes \sum_{i=1}^N \alpha_i |i\rangle |d_i\rangle$$

*where each  $d_i$  is an arbitrary  $m$ -bit binary string. Then the quantum circuit implementing  $U$  must have at least  $\mathcal{O}(Nm)$  elementary gates.*

*Proof.* Since all  $d_i$  strings are arbitrary, we can prove the result using the counting argument. The classical data to be loaded can be considered as a dictionary  $\{(i, d_i) | i \in [N]\}$ , which contains  $Nm$  bits in total. The total number of possible dictionaries is therefore  $2^{Nm}$ . The unitary  $U$  must be able to distinguish between all  $2^{Nm}$  possibilities. If  $U$  is composed of an elementary gate set in which each gate acts on a constant number of qubits, then the number of gates required to distinguish  $2^{Nm}$  cases is  $\log(2^{Nm}) = \mathcal{O}(Nm)$ .  $\square$

Previous results [12, 89, 8] suggested different architectures to implement QROM with different trade-offs between circuit depth and width. In Appendix C, we propose a new scheme of QROM by direct quantization of classical Read-Only Memory with logarithmic depth and a width-depth tradeoff feature.

However, as [62] points out, asymptotic advantages of quantum algorithms in time complexity may also be affected by circuit-based active QROM/QRAM. This is because the number of (logical) qubits involved in a QRAM/QROM circuit is at least  $\Omega\left(\frac{N}{\log N}\right)$ , which requires a significant amount of effort in classical control. Since controlling a logical qubit is difficult, the classical controlling resources required can be considered as  $\Omega\left(\frac{N}{\log N}\right)$  parallel processors. When so many processors are used, it is possible that a classical parallel algorithm can solve the same computational problem in a comparable amount of time. However, we argue that as experimental techniques evolve, classical control of qubits will become less challenging such that  $\frac{N}{\log N}$  qubits require a comparable amount of control as  $\frac{N}{\log N}$  classical bits, much less than  $\frac{N}{\log N}$  parallel classical computers. In this case, an exponential speedup in time complexity is a significant improvement over classical computation. For instance, in Ref. [22], an experimental platform based on reconfigurable atom array features collective control of a set of physical qubits composing a logical qubit. Although there is still a significant amount of effort to control each logical qubit, it is hopeful for future devices to use much fewer classical control lines. In such a case, the classical co-processors should not be considered as a large parallel computer. We also notice that [1] if fan-in gates can be implemented in some experimental platforms, then circuit depth for QRAM/QROM can even be reduced to a constant, even though qubit number required still scales linearly in the amount of data.

### 3 Protein dynamics

A direct approach to simulating the dynamics of proteins, especially their conformational changes, is by solving Newton's equations that govern the motion of the constituent atoms,

$$m_i \frac{d^2}{dt^2} \mathbf{u}_i = -\nabla_{R_i} V(\mathbf{u}_1, \mathbf{u}_2, \dots, \mathbf{u}_N). \quad (3.1)$$

Here  $\mathbf{u} \in \mathbb{R}^n$  is the displacement vector. This method, later known as molecular dynamics (MD), gained prominence as models for  $V$  describing interatomic interactions, also known as the force field [70], become more accurate and available [87, 79]. Numerous computational techniques have been extensively developed to enhance computational efficiency, e.g., computing long-range interactions and long-time integration, and to accurately model the physical conditions under which these



dynamics occur [48, 95]. However, the considerable disparity between the time scales of molecular movements ( $10^{-15}$ s) and those of conformational changes (at least  $10^{-3}$ s), coupled with the vast number of atoms involved, necessitates massive computing power to directly simulate protein dynamics [68].

### 3.1 Normal mode models

As a first step toward achieving advantage in simulating protein dynamics, we consider the model class of normal mode dynamics, which works in the harmonic approximation regime in which the equations of motion (3.1) are simplified to,

$$M \frac{d^2}{dt^2} \mathbf{u} = -K\mathbf{u}. \quad (3.2)$$

Here  $\mathbf{u} \in \mathbb{R}^n$  is a vector containing the displacement of a component of the protein. The component may refer to an atom, a residue, or a rigid cluster.  $M \in \mathbb{R}^{n \times n}$  is a diagonal matrix that contains the mass of the components. Meanwhile,  $K \in \mathbb{R}^{n \times n}$ , known as the stiffness matrix, is a symmetric semi-positive definite matrix with elements representing the interactions in the protein.

The method for predicting protein dynamics based on (3.2) is known as the normal mode analysis (NMA). Despite the simplicity of the model, NMA has demonstrated its ability to efficiently predict vibration modes that correlate well with large-scale conformation changes of proteins [14], and has played a key role in many simulation-based studies as well as coarse-graining methods [71, 98, 45].

Meanwhile, in biomolecular simulations, NMA models have been developed with varying levels of resolution and complexity. The core assumption of NMA is that any given equilibrium system fluctuates about a single well-defined conformation and that the nature of these thermally induced fluctuations can be calculated assuming a simple harmonic form for the potential. Specifically, a protein in NMA is represented by a collection of nodes, here labeled by  $i \in [N] := \{1, 2, \dots, N\}$ . Further, we denote the instantaneous position of the  $i$ -th node by  $R_i$  with equilibrium position  $R_i^0$ . Therefore the dynamics are reflected in the displacement vector  $\mathbf{u}_i = R_i - R_i^0$ . Here we give brief overview of such models

- **Harmonic approximation of the full MD model (3.1)**. In this case, the stiffness matrix  $K$  is obtained directly from the Hessian of the interatomic potential.
- **Gaussian network model (GNM) [14, 54]**. The GNM only works with the  $C^\alpha$  atoms and is built on the assumption that the relative distance between  $C^\alpha$  atoms follows a Gaussian distribution.
- **The Anisotropic Network Model (ANM) [10]**. ANM is an extension of GNM, in that it includes all three coordinates of the displacement of each  $C^\alpha$  atom, thus accounting for directional movements.

- **All-atom NMA** [49]. These models involve all the atoms in the protein. However, the elements of the stiffness matrix  $K$  are specified based on the interatomic distance and bond type.

For readers interested in a more detailed discussion of existing normal mode models, please refer to Appendix A.

### 3.2 Normal mode dynamics with external effects

Solvent molecules, typically water, interact with the protein’s surface through hydrogen bonding and hydrophobic interactions, which may directly impact the protein’s conformation. A simple way to model the effect of solvent molecules is by Langevin dynamics, which after the harmonic approximation of the inter-molecular forces, leads to the linear stochastic differential equation

$$M \frac{d^2 \mathbf{u}}{dt^2} = -\gamma \frac{d\mathbf{u}}{dt} - K\mathbf{u} + \xi(t). \quad (3.3)$$

Here  $\gamma$  is a friction coefficient and it provides velocity-dependent damping. Meanwhile, the white noise  $\xi$  accounts for thermal energy transferred to the molecule from the solvent. The elements of this vector obey the properties

$$\mathbb{E}[\xi_i(t)] = 0 \quad (3.4)$$

and the fluctuation-dissipation theorem,

$$\mathbb{E}[\xi_i(t)\xi_j(t')] = 2\gamma k_B T \delta_{ij} \delta(t - t'). \quad (3.5)$$

### 3.3 Steered Protein Dynamics

Another simple extension is the normal mode dynamics under a mechanical force,

$$M \frac{d^2 \mathbf{u}}{dt^2} = -K\mathbf{u} + \mathbf{f}(t), \quad (3.6)$$

where  $\mathbf{f}(t)$  can be regarded as a mechanical load.

This idea has been pursued in the steered MD approach [61], where the forces are used to speed up the folding process. Similarly, Arkun and Gur considered the driven dynamics (3.6) in an optimal control framework, where  $\mathbf{f}(t)$  involves control variables that are determined by minimizing a cost function.

## 4 Initial state preparation

To simulate molecular dynamics using the [11] algorithm, the initial quantum state fed into the algorithm must represent the initial state of the high-dimensional coupled oscillator system of the corresponding model of protein. Recall that  $N$  is the number of oscillators (atoms, residues, etc.)

in the protein dynamical system. Our quantum algorithm needs  $n = \mathcal{O}(\log N)$  qubits to simulate its dynamics. Regardless of which model we use, the initial state should be of the following form:

$$|\psi(0)\rangle := \frac{1}{\sqrt{2E}}[\dot{\mathbf{y}}(0), i\sqrt{A}\mathbf{y}(0)]^T, \quad (4.1)$$

where  $\mathbf{y}(0) = \sqrt{M}\mathbf{u}(0)$  and  $A := (\sqrt{M})^{-1}K(\sqrt{M})^{-1}$ . Once the initial state is prepared, we can use [11, Lemma 9] to generate  $|\psi(t)\rangle$  which encodes the final state of the protein dynamical system. Note that  $|\psi(0)\rangle$  (and  $|\psi(t)\rangle$ ) is the amplitude encoding of the dynamical state: the (relative) displacement and velocity of any component (which may be a residue or a single atom) in the system is encoded as the amplitude corresponding to the component's index.

Observe that initial displacements and initial velocities are represented by amplitudes of non-overlapping sets of values in the register. We can show that if we are able to prepare the states proportional to the initial displacements and initial velocities respectively and are given oracle access to both the  $M$  and  $K$  matrices, then the initial state can be prepared efficiently.

**Lemma 4.1** (Joint state preparation from [11]). *Assume we have access to the oracle  $\mathcal{S}$  for  $d$ -sparse kernel matrix  $H$  and diagonal mass matrix  $M$ , and the unitary  $U_I$  that performs the map*

$$U_I |0\rangle |0\rangle = |0\rangle |\dot{\mathbf{u}}(0)\rangle, \quad U_I |1\rangle |0\rangle = |1\rangle |\mathbf{u}(0)\rangle, \quad (4.2)$$

where

$$|\mathbf{u}(0)\rangle \propto \sum_{j=1}^N \mathbf{u}_j(0) |j\rangle, \quad |\dot{\mathbf{u}}(0)\rangle \propto \sum_{j=1}^N \dot{\mathbf{u}}_j(0) |j\rangle, \quad (4.3)$$

are normalized states. There exists a quantum algorithm that prepares the state

$$|\psi(0)\rangle := \frac{1}{\sqrt{2E}}[\dot{\mathbf{y}}(0), i\sqrt{A}\mathbf{y}(0)]^T, \quad (4.4)$$

where  $\mathbf{y}(0) = \sqrt{M}\mathbf{u}(0)$  and  $A := (\sqrt{M})^{-1}K(\sqrt{M})^{-1}$ , and  $E$  is the total energy. The quantum circuit makes  $Q_{\text{ini}} = \mathcal{O}(\frac{E_{\text{max}}d}{E})$  uses of  $\mathcal{S}$ ,  $U_I$ , and its inverses, in addition to

$$G_{\text{ini}} = \mathcal{O}\left(\frac{E_{\text{max}}d}{E} \text{polylog}\left(\frac{NE_{\text{max}}d}{E\epsilon}\right)\right) \quad (4.5)$$

two-qubit gates. Here  $E_{\text{max}} := \frac{m_{\text{max}}}{2} \sum_j (\dot{\mathbf{u}}_j(0))^2 + \frac{\kappa_{\text{max}}}{2} \sum_j (\mathbf{u}_j(0))^2$ .

As for other models, we might start by obtaining samples from the *uniform distribution* of displacements and velocities, or even using the Rotation Translational Block (RTB) method as introduced in Section 7.2 with more details.

## 4.1 Gaussian random amplitude states

Now that Lemma 4.1 holds, it suffices to know how to implement  $U_I$ , which is determined by the model of protein dynamics. In this subsection, we focus on the Gaussian network model, in which all initial displacements and initial velocities follow some *Gaussian distributions* independently.

In particular, all coefficients of the displacement state  $|\mathbf{u}(0)\rangle$  and velocity state  $|\dot{\mathbf{u}}(0)\rangle$  should be random variables with zero mean, and  $\mathbf{u}_j(0)$  and  $\dot{\mathbf{u}}_j(0)$  independently follows a real Gaussian distribution  $\mathcal{N}(0, \mu)$  with rescaling to a unit vector. This implies that Gaussian network model requires this distribution of initial states, which is a different notion than conventional initial states that represent distributions.

To address the problem of sampling and preparing these states, we first identify two classes of initial state preparation problems for two different computational tasks. We define the first kind of task, called *ensemble simulation*, as computing the average behavior of the system over the distribution of all possible input states. In this case, the initial state should be *sampled* from the Gaussian distribution, as described in the following problem.

**Problem 1** (Initial state preparation for ensemble simulation in Gaussian network model). *We need to prepare a mixed state  $\rho_G$  defined as the convex combination of all Gaussian random amplitude states weighted by their probability densities.*

An in-depth study of the protein dynamical system under one specific random initial condition may also be useful for biology and chemistry. For instance, one may be interested in the evolution of a single initial state, which requires multiple times of simulations under the same initial state. One may also study how the properties and dynamics of the system change when a small perturbation or modification is applied to the initial state, which requires the capability of fine-tuning the initial state preparation procedure to produce a slightly different initial state deterministically. These features above may also be useful when studying a class of randomized simulation and their path dependence. We call this situation *single-state simulation*, where the initial state is one specific reproducible Gaussian random (or pseudo-random) state sampled from its distribution. We define the initial state preparation problem for single-state simulation as follows.

**Problem 2** (Initial state preparation for single-state simulation in Gaussian network model). *We need to (pseudo-)randomly sample one Gaussian random amplitude state (representing  $|\mathbf{u}(0)\rangle$  or  $|\dot{\mathbf{u}}(0)\rangle$ ) and prepare it. We also need to reproduce this specific Gaussian random amplitude state arbitrarily many times.*

#### 4.1.1 Initial state preparation for ensemble simulation.

To solve Problem 1, our first finding is the following lemma.

**Lemma 4.2** (Distribution of Gaussian random amplitude states). *Gaussian random amplitude states corresponding to any uncertainty  $\mu > 0$  follow the same uniform distribution of real-amplitude states.*

*Proof.* We notice that one sample of *unnormalized* Gaussian random amplitude state of  $n$  qubits with uncertainty  $\mu$  can be represented by an array of  $2^n$  real numbers, denoted by  $\boldsymbol{\alpha} = (\alpha_0, \dots, \alpha_{2^n-1})^T$ , with  $\alpha_i \sim \mathcal{N}(0, \mu)$  for all  $i$ . The unnormalized state corresponding to  $\boldsymbol{\alpha}$  is

$$|\psi_{\boldsymbol{\alpha}}\rangle = \sum_{i=0}^{2^n-1} \alpha_i |i\rangle. \quad (4.6)$$

The probability density corresponding to  $|\psi_{\alpha}\rangle$  is

$$f(|\psi_{\alpha}\rangle) = \prod_{i=0}^{2^n-1} \frac{1}{\sqrt{2\pi\mu^2}} \exp\left(-\frac{\alpha_i^2}{2\mu^2}\right) = (2\pi\mu^2)^{-2^{n-1}} \exp\left(-\frac{1}{2\mu^2} \sum_{i=0}^{2^n-1} \alpha_i^2\right). \quad (4.7)$$

The normalized version of  $|\psi_{\alpha}\rangle$  is simply  $|\tilde{\psi}_{\alpha}\rangle := \frac{1}{\sqrt{\sum_{i=0}^{2^n-1} \alpha_i^2}} |\psi_{\alpha}\rangle$ . We then observe that the probability density corresponding to  $|\tilde{\psi}_{\alpha}\rangle$  is a value depending only on  $\mu$ :

$$f(|\tilde{\psi}_{\alpha}\rangle) = (2\pi\mu^2)^{-2^{n-1}} \exp\left(-\frac{1}{2\mu^2} \sum_{i=0}^{2^n-1} \frac{\alpha_i^2}{\sum_{j=0}^{2^n-1} \alpha_j^2}\right) = (2\pi\mu^2)^{-2^{n-1}} e^{-\frac{1}{2\mu^2}}. \quad (4.8)$$

Therefore, any unnormalized version of  $|\psi_{\alpha}\rangle$  can be written as  $\gamma |\tilde{\psi}_{\alpha}\rangle$  with  $\gamma \neq 0$  and has probability density

$$f(\gamma |\tilde{\psi}_{\alpha}\rangle) = (2\pi\mu^2)^{-2^{n-1}} e^{-\frac{\gamma^2}{2\mu^2}}. \quad (4.9)$$

The probability density of all states equivalent to  $|\psi_{\alpha}\rangle$  can also be calculated by integrating over  $\gamma \in (-\infty, 0) \cup (0, \infty)$  since  $\gamma = 0$  is forbidden:

$$\Pr(|\psi_{\alpha}\rangle) = \int_{\gamma=-\infty}^{\infty} f(\gamma |\tilde{\psi}_{\alpha}\rangle) (1 - \delta(\gamma)) d\gamma = \int_{\gamma=-\infty}^{\infty} (2\pi\mu^2)^{-2^{n-1}} (1 - \delta(\gamma)) e^{-\frac{\gamma^2}{2\mu^2}} d\gamma \quad (4.10)$$

which is again a value independent of  $\alpha$ . This implies that the probability of obtaining any  $|\tilde{\psi}_{\alpha}\rangle$  from the distribution of Gaussian random amplitude states is the same. Therefore, the distribution of Gaussian random amplitude states is simply the uniform distribution of all real-amplitude normalized states.  $\square$

Letting  $p := \Pr(|\psi_{\alpha}\rangle)$  and using the fact that  $|\psi_{\alpha}\rangle$  is normalized when  $\sum_{i=0}^{2^n-1} \alpha_i^2 = 1$ , we can write down the density matrix describing the distribution of initial states and decompose it in the computational basis:

$$\begin{aligned} \rho_G &= \int_{\sum_{i=0}^{2^n-1} \alpha_i^2=1} \Pr(|\psi_{\alpha}\rangle) |\psi_{\alpha}\rangle \langle \psi_{\alpha}| d\alpha \\ &= p \left[ \sum_{j=0}^{2^n-1} \int_{\sum_{i=0}^{2^n-1} \alpha_i^2=1} \alpha_j^2 |j\rangle \langle j| d\alpha + \sum_{j,k=0}^{2^n-1} \int_{\sum_{i=0}^{2^n-1} \alpha_i^2=1} \alpha_j \alpha_k |j\rangle \langle k| d\alpha \right] \\ &= \frac{1}{2^n} \sum_{j=0}^{2^n-1} |j\rangle \langle j| \end{aligned} \quad (4.11)$$

where all non-diagonal terms have 0 amplitude in the density matrix since  $\alpha_j \alpha_k$  is an odd function when integrating over any of them, and all diagonal terms have equal weight since  $\int_{\sum_{i=0}^{2^n-1} \alpha_i^2=1} \alpha_j^2$  is the same for all  $j$ .

Therefore, if we wish to compute any average quantity over all possible initial states, it suffices to prepare the maximally mixed state by preparing

$$|\psi_{\text{pure}}\rangle = \frac{1}{\sqrt{2^n}} \sum_{j=0}^{2^n-1} |j\rangle |j\rangle \quad (4.12)$$

and discarding the second register.  $|\psi_{\text{pure}}\rangle$  can be easily prepared by performing Hadamard gates on all qubits and applying CNOT gates between qubits in register 1 and register 2. We summarize our result as the following theorem.

**Theorem 4.3** (Initial state preparation for ensemble simulation). *The initial states for ensemble simulation of  $n$  qubits can be prepared using a depth-2 circuit on  $2n$  qubits.*

Furthermore, we notice that a  $|\psi_{\text{pure}}\rangle$  is the purification of  $\rho_G$ , which can also be used to estimate average quantities over the ensemble, as shown below. Let  $U$  be the quantum simulation algorithm and  $O$  be the observable to be measured. The expectation value of  $O$  over the whole ensemble of Gaussian random amplitude states is

$$\text{Tr}[U\rho_G U^\dagger O] = \frac{1}{2^n} \sum_{j=0}^{2^n-1} \langle j|U^\dagger O U|j\rangle. \quad (4.13)$$

Now, if we run  $I \otimes U$  on  $|\psi_{\text{pure}}\rangle$  and measure  $I \otimes O$ , we obtain

$$\text{Tr}[I \otimes U \cdot |\psi_{\text{pure}}\rangle \langle \psi_{\text{pure}}| \cdot I \otimes U^\dagger \cdot I \otimes O] = \frac{1}{2^n} \sum_{j=0}^{2^n-1} \langle j|j\rangle \langle j|U^\dagger O U|j\rangle = \text{Tr}[U\rho_G U^\dagger O], \quad (4.14)$$

which is the same mean value. Note that we have access to both the circuit preparing  $U|\psi_{\text{pure}}\rangle$  and its reverse. This implies that we can employ *quantum mean estimation* [25, 35, 55] to achieve a quadratic improvement in the sample complexity of estimating any average value over the whole distribution.

### 4.1.2 Single Gaussian random amplitude state preparation

To solve Problem 2, it does not suffice to only prepare  $\rho_G$ . Instead, we need to generate sample states representing physically non-trivial initial configurations of the dynamical system, which is the state  $|\psi_{\alpha}\rangle$  where  $\alpha$  satisfies the Gaussian randomness condition and normalization condition. Most oscillators in this kind of initial state should have close-to-zero (but non-zero) displacements and velocities. Moreover, if the random state is sampled by measuring a larger quantum state, then it might be difficult to generate the same state again or slightly modify the generated state, due to the no-cloning theorem and the large overhead of post-selection. Therefore, we prefer to generate the randomness using classical approaches, meaning that the state is pseudo-random rather than true random. Note that true randomness is not necessary for our purpose because we only aim to achieve the same outcomes of protein dynamics simulation as classical approaches, and scientists only have access to pseudo-randomness with classical computers.

The most conceptually simple method is to first sample an  $\alpha$  array classically using pseudo-random generators, then normalize it and design a quantum circuit to prepare  $|\psi_\alpha\rangle$ . However, this approach requires transmitting  $\mathcal{O}(2^n)$  bits into the quantum circuit and implementing  $\mathcal{O}(2^n)$  gates, which is inefficient for large  $n$ . To address this problem, we devise a new algorithm for preparing Gaussian pseudo-random amplitude states based on the Gaussian random amplitude loading approach introduced in Section 4.1 of [24].

**Theorem 4.4** (Gaussian pseudo-random amplitude state preparation). *A single Gaussian pseudo-random amplitude state of  $n$  qubits can be generated deterministically using  $\text{poly}(n)$  quantum gates and  $\text{poly}(n)$  classical bits which are used as the source of randomness.*

We describe our method as follows. Our approach uses binary data loaders extensively, the same as in Ref. [24]. A binary data loader  $L_h$  parametrized by angles  $\theta = (\theta_0, \theta_1, \dots, \theta_{2^n-1})$  acting on the  $l$ th qubit implements the following operation

$$L_l(\theta) : |i\rangle |0\rangle \rightarrow \cos(\theta_i) |i\rangle |0\rangle + \sin(\theta_i) |i\rangle |1\rangle \quad (4.15)$$

where  $i$  is an integer represented by a binary string of  $l-1$  bits, and  $\theta_i \in [0, \pi/2]$ . In fact, any  $n$ -qubit state  $|\phi\rangle = \sum_j \beta_j |j\rangle$  with  $\beta_j \in \mathbb{R}$  can be prepared using  $n$  binary data loaders: if  $\theta_i$  is computed by

$$\cos(\theta_i) = \frac{\sum_{j \in \{0,1\}^{n-l}} |\beta_{i0j}|^2}{\sum_{k \in \{0,1\}^{n-l+1}} |\beta_{ik}|^2}, \quad (4.16)$$

then one can prepare  $|\phi\rangle$  by applying each  $L_l$  with  $l \in \{1, 2, \dots, n\}$  sequentially. Since  $\theta$  has  $\mathcal{O}(2^n)$  elements, it is expensive to compute all  $\theta_i$  values classically and communicate them to the quantum circuit. We instead choose to generate  $\theta$  directly by the quantum circuit itself. For Gaussian random amplitude states, the following lemma from [24] gives a hint for how to generate these angles.

**Lemma 4.5** (Lemma 4.8 of [24]). *The  $n$ -qubit quantum state  $|\psi_\alpha\rangle$  where  $\alpha_i$  are independent  $\mathcal{N}(0, 1)$  random variables can be prepared using the binary data loader construction with angles  $\theta_i$  at the  $l$ th qubit distributed independently according to the density function*

$$p_l(\theta_i) \propto \sin^{2^{n-l}-1}(\theta_i) \cos^{2^{n-l}-1}(\theta_i) \propto \sin^{2^{n-l}-1}(2\theta_i).$$

Now, to produce one Gaussian random amplitude state, we need to sample all  $\theta_i$  angles according to the distribution above. The approach in Ref. [24] is to prepare another state

$$|\psi_\theta\rangle \propto \sum_{\theta} \sqrt{\prod_{l=1}^n \prod_{i \in \{0,1\}^{l-1}} p_l(\theta_i)} |\theta\rangle \quad (4.17)$$

which can be done using the Grover-Rudolf algorithm [53] in  $\mathcal{O}(n)$  depth. However, this method gives true random states, does not allow for reproducing the same random state, and is qubit-consuming since it takes  $\mathcal{O}(2^n)$  qubits to store the whole  $\theta$ .

To address the issues above, our plan is to sample  $\theta_i$  for all  $i$  with  $l$  bits *coherently* and *deterministically* before applying the  $l$ th binary data loader. In other words, we need to design a reversible classical circuit for generating a pseudo-random sample of  $\theta_i$  for any  $i$  of  $l$  bits, without knowing the value of any  $\theta_j$  with  $j \neq i$  (such that all  $\theta_i$ s can be generated in parallel), and transform it into a quantum circuit.

We propose two algorithms to solve this problem, and both are based on counter-based pseudo-random number generators (CBRNG), some non-recursive random number generators.

**Definition 4.6** (CBRNG). An  $n$ -bit CBRNG is an efficiently computable (i.e., in  $\text{poly}(n)$  time) function which for all  $i \in \{0, 1, \dots, 2^n - 1\}$  satisfies

$$\text{CBRNG}(s, i) = r_{s,i} \quad (4.18)$$

where  $s \in \{0, 1, \dots, 2^{\text{poly}(n)} - 1\}$  is a random seed, and  $r_{s,i}$  is a pseudo-random number sampled from the uniform distribution of  $\{0, 1, \dots, \max(r)\}$  with  $\max(r) \leq 2^{\text{poly}(n)}$ .

An example of CBRNG is the *counter mode of block cipher* method, whose basic idea is to encode the index  $i$  by permuting its bits corresponding to the seed. More CBRNG proposals can be found in Refs. [94, 101]. Since CBRNGs are classical deterministic procedures, one can always produce the same  $r_{s,i}$  values if a fixed seed  $s$  is chosen.

We present both algorithms of generating  $\theta$  as follows.

**Algorithm 1 (naive).** CBRNG enables a straightforward (but not necessarily efficient) sampling method for  $\theta_i$ s based on inverting the cumulative distribution function, which is described as follows. Without loss of generality, let us consider the data loader acting on the  $l$ th qubit, which has  $2^{l-1}$  possible input values, i.e., the state at this step is  $|\psi_l\rangle = \sum_{i \in \{0,1\}^{l-1}} \alpha_{l,i} |i\rangle$  with  $\sum |\alpha_{l,i}|^2 = 1$ . For all  $i$  in this superposition, we need to generate their corresponding  $\theta_i$ s simultaneously. First, we choose the random seed  $s$  and compute  $r_{s,i}$  using the CBRNG for each  $i$  in superposition. More specifically, let the state prior to the  $l$ th binary data loader be  $\sum_{i \in \{0,1\}^{l-1}} \alpha_{l,i} |i\rangle$ , then the (quantized) CBRNG gives

$$\sum_{i \in \{0,1\}^{l-1}} \alpha_{l,i} |i\rangle |0\rangle \mapsto \sum_{i \in \{0,1\}^{l-1}} \alpha_{l,i} |i\rangle |r_{s,i}\rangle. \quad (4.19)$$

Then, a random  $\theta_i$  can be generated from  $r_{s,i}$  if we can invert the cumulative distribution function of  $\theta_i$ , i.e. computing the value  $\theta_i$  such that

$$\int_0^{\theta_i} p_l(x) dx = \frac{r_{s,i}}{\max(r)}. \quad (4.20)$$

If this can be done efficiently, then the following operation can be implemented efficiently:

$$\begin{aligned} \sum_{i \in \{0,1\}^{l-1}} \alpha_{l,i} |i\rangle |r_{s,i}\rangle |0\rangle &\mapsto \sum_{i \in \{0,1\}^{l-1}} \alpha_{l,i} |i\rangle |r_{s,i}\rangle |\theta_i\rangle \\ &\mapsto \sum_{i \in \{0,1\}^{l-1}} \alpha_{l,i} (\cos(\theta_i) |i0\rangle + \sin(\theta_i) |i1\rangle) |r_{s,i}\rangle |\theta_i\rangle \\ &\mapsto \sum_{i \in \{0,1\}^{l-1}} \alpha_{l,i} (\cos(\theta_i) |i0\rangle + \sin(\theta_i) |i1\rangle) |0\rangle |0\rangle \end{aligned} \quad (4.21)$$



where we employ the binary data loader in the second line and use the reversibility of the quantum circuit in the last line. Now, the binary data loader does not need to query all  $\theta_i$  angles stored in an independent register, because they can be generated whenever they are needed. Since we only need one ancilla register to store  $\theta_i$ s and it can be reused by the next data loader, we only need  $\text{poly}(n)$  ancilla qubits to store the seed, instead of  $\mathcal{O}(2^n)$  qubits for the whole  $\boldsymbol{\theta}$  vector. The gate complexity of the whole process is also  $\text{poly}(n)$ .

However, it is unclear if the integration in Equation (4.20) can be efficiently computed for  $l \ll n$ , thus inverting the cumulative distribution function might require numerical integration approaches and Newton's iterative method. We leave it as an open problem to find and quantize the best method for inverting the cumulative distribution function and analyzing its resource requirements.

**Algorithm 2 (rejection sampling).** To circumvent the hardness of inverting the cumulative distribution function, we design the second algorithm based on classical *rejection sampling* to generate  $\theta_i$ . Rejection sampling is a widely used approach in classical computation to sample from hard-to-sample-from distributions, which we outline as follows. For a target distribution  $p_l(x)$ , we need to first find a proposal distribution  $q(x)$  which is easy to sample from (for instance, the cumulative distribution function of  $q(x)$  may be efficiently invertible), and a real number  $Q$  such that  $Qq(x) \geq p(x)$  for all  $x$ . Then, we generate a sample  $s_q$  from  $q(x)$  and a random number  $r_q$  uniformly from  $[0, Qq(s_q)]$ . Next, if  $r_q \leq p(s_q)$ , then  $s_q$  is accepted as a sample from  $p(x)$ ; otherwise,  $s_q$  is abandoned. The success probability of obtaining one sample using this approach is  $p_{\text{suc}} := \frac{\int p(x)dx}{\int Qq(x)dx}$ , therefore, it is key to choose an appropriate  $Qq(x)$  that it is sufficiently close to  $p(x)$ .

Our quantum approach is the quantization of the classical rejection sampling with the help of CBRNGs. Before describing the quantum circuit, we need to find the proposal distribution  $q_l$  for each  $l$ , and the  $Q_l$  factor to guarantee  $Q_l q_l(x) \geq p_l(x)$ . Indeed, we can show that such a proposal distribution exists. We notice that for  $n - l \lesssim \log n$ , sampling from  $p_l(\theta_i)$  is not difficult, since  $\int p_l(x)dx$  can be written analytically using  $\text{poly}(n)$  terms. Therefore, we focus on the case where  $n - l \gg \log n$ .

**Lemma 4.7** (Proposal distribution). *For  $l' := n - l \gg \log n$ , there exists a  $Q_l \in \mathbb{R}$  and a proposal distribution  $q_l(x)$  for every  $l < n$  such that rejection-sampling success probability  $p_{\text{suc},l} = \mathcal{O}(1)$  and  $q_l(x)$  can be efficiently sampled from by inverting its cumulative distribution function using pseudo-random numbers.*

*Proof.* We first write  $p_l(\theta_i)$  as

$$p_l(\theta_i) = \frac{1}{\zeta_l} \sin^{2^{l'}-1}(2\theta_i) \quad (4.22)$$

where the normalization factor  $\zeta_l$  can be computed by integrating  $\sin^{2^{l'}-1}(x)$ :

$$\zeta_l = \int_0^{\pi/2} \sin^{2^{l'}-1}(2x)dx = \frac{1}{2} \int_0^{\pi} \sin^{2^{l'}-1}(x)dx = 2^{2^{l'}-l'-1} \left[ \binom{2^{l'}}{2^{l'}-1} \right]^{-1}. \quad (4.23)$$

Recall that we focus on the case of  $l' \gg \log n$ . Using

$$\frac{2^{2l'}}{\sqrt{\pi(2^{l'-1} + \frac{1}{3})}} \leq \binom{2^{l'}}{2^{l'-1}} \leq \frac{2^{2l'}}{\sqrt{\pi(2^{l'-1} + \frac{1}{4})}}, \quad (4.24)$$

we can rewrite  $\zeta_l$  as

$$\zeta_l = \sqrt{\pi} \cdot 2^{-l'-1} \cdot \left( 2^{\frac{l'-1}{2}} + \mathcal{O}\left(2^{\frac{-l'+1}{2}}\right) \right) = 2^{\frac{-l'-3}{2}} \sqrt{\pi} + \mathcal{O}\left(2^{\frac{-3l'}{2}}\right). \quad (4.25)$$

We use a step function (piecewise constant function) to construct  $Q_l \cdot q_l(x)$ . Since  $p_l(x)$  is peaked at  $x = \pi/4$ , we let  $Q_l \cdot q_l(x) = p_l(\pi/4) = \zeta_l^{-1}$  in a small region around  $x = \pi/4$ . We choose the region to be  $[\pi/4 - \zeta_l, \pi/4 + \zeta_l]$ . One can now see that

$$\int_{\pi/4 - \zeta_l}^{\pi/4 + \zeta_l} Q_l \cdot q_l(x) dx = 2, \quad (4.26)$$

while

$$\begin{aligned} \int_{\pi/4 - \zeta_l}^{\pi/4 + \zeta_l} p_l(x) dx &\geq 2\zeta_l \cdot p_l(\pi/4 - \zeta_l) \\ &= 2 \sin^{2^{l'} - 1}(\pi/2 - 2\zeta_l) \\ &= 2 \left[ 1 - 2\zeta_l^2 + \frac{2}{3}\zeta_l^4 - \dots \right]^{2^{l'} - 1} \\ &= 2 \left[ 1 - \frac{\pi}{4} 2^{-l'} + \mathcal{O}(2^{-2l'}) \right]^{2^{l'} - 1} \\ &\geq 2 \left[ 1 - \frac{\pi}{4} 2^{-l'} \right]^{2^{l'} - 1} \\ &= 2e^{-\pi/4} + \mathcal{O}(2^{-l'}) \approx 0.91 + \mathcal{O}(2^{-l'}) \end{aligned} \quad (4.27)$$

which is a constant close to 1 when  $l'$  is large. In this range, our  $Q_l \cdot q_l(x)$  performs well, since the ratio between the integral of the real distribution and the proposal distribution is at least 0.45 when  $l'$  is large.

Next, we construct  $Q \cdot q_l(x)$  in the region to the left side of  $\pi/4 - \zeta_l$  and to the right side of  $\pi/4 + \zeta_l$ . We consider the range  $x \in [\pi/4 - 2\zeta_l, \pi/4 - \zeta_l] \cup [\pi/4 + \zeta_l, \pi/4 + 2\zeta_l]$  and simply let  $Q_l \cdot q_l(x) = p_l(\pi/4 - \zeta_l)$  for  $x$  in this range. Similarly, the  $k$ th region to consider is  $x \in [\pi/4 - k\zeta_l, \pi/4 - (k-1)\zeta_l] \cup [\pi/4 + (k-1)\zeta_l, \pi/4 + k\zeta_l]$ , and the value of  $Q_l \cdot q_l(x)$  is  $p_l(\pi/4 - (k-1)\zeta_l)$ . We proceed to increase  $k$  one by one, until we reach  $k = k_T$  satisfying  $p_l(\pi/4 - k_T\zeta_l) = \mathcal{O}(2^{-l'})$ . Since that the probability of obtaining  $x \in [0, \pi/4 - k_T\zeta_l]$  is exponentially small, we can simply let  $Q_l q_l(x) = p_l(\pi/4 - k_T\zeta_l)$  for  $x \in [0, \pi/4 - k_T\zeta_l] \cup [\pi/4 + k_T\zeta_l, \pi/2]$ . We can compute  $k_T$  by

$$p_l(\pi/4 - k_T\zeta_l) = \frac{1}{\zeta_l} \left[ 1 - \frac{k^2\pi}{4} 2^{-l'} \right]^{2^{l'} - 1} = \mathcal{O}\left(2^{\frac{l'}{2}} e^{-\frac{k^2\pi}{4}}\right) \leq \mathcal{O}(2^{-l'}) \quad (4.28)$$

which implies that  $k_T = \mathcal{O}(\sqrt{l}) = \mathcal{O}(\sqrt{n})$ . Therefore,  $Q_l q_l(x)$  is efficiently computable, integrable, and its integration is efficiently invertible, since  $Q_l q_l(x)$  is a step function of at most  $\mathcal{O}(\sqrt{n})$  steps.

Finally, we compute the success probability of rejection sampling,  $p_{\text{suc},l}$ , which is related to the area enclosed by  $Q_l p_l(x)$ . We first compute an upper bound of the area enclosed by it in the  $k$ th range, i.e.,  $[\pi/4 - k\zeta_l, \pi/4 - (k-1)\zeta_l] \cup [\pi/4 + (k-1)\zeta_l, \pi/4 + k\zeta_l]$ :

$$\begin{aligned}
2 \int_{\pi/4 - k\zeta_l}^{\pi/4 - (k-1)\zeta_l} Q \cdot q_l(x) dx &= 2\zeta_l q_l(\pi/4 - (k-1)\zeta_l) \\
&= 2 \left[ 1 - \frac{(k-1)^2 \pi}{4} 2^{-l'} + \mathcal{O}(2^{-2l'}) \right]^{2^{l'} - 1} \\
&\leq 2 \left[ 1 - \frac{(k-1)^2 \pi}{2} 2^{-l'} + \mathcal{O}(2^{-2l'}) \right]^{2^{l'} - 1} \\
&= e^{-\frac{(k-1)^2 \pi}{2}} + \mathcal{O}(2^{-l'}).
\end{aligned} \tag{4.29}$$

Therefore, the total area can be upper bounded by

$$\int_0^{\pi/2} Q_l p_l(x) dx \leq 2 \sum_{k=1}^{\mathcal{O}(\sqrt{n})} e^{-\frac{(k-1)^2 \pi}{2}} = \mathcal{O}(1), \tag{4.30}$$

a constant. This implies that the rejection sampling success probability satisfies

$$p_{\text{suc},l} = \frac{\int_0^{\pi/2} p_l(x) dx}{\int_0^{\pi/2} Q_l p_l(x) dx} \geq \mathcal{O}(1). \tag{4.31}$$

□

Now, without loss of generality, we again outline the quantum algorithm for the  $l$ th data loader. We use two random seeds,  $s$  and  $s'$ . We first generate a pseudo-random number  $r(s, i)$  using CBRNG, then invert the cumulative distribution function of  $q_l(x)$  to obtain  $s_q(i)$  which is a sample from  $q_l(x)$  corresponding to the random number  $r(s, i)$ :

$$\begin{aligned}
\sum_{i \in \{0,1\}^{l-1}} \alpha_{l,i} |i\rangle |00 \dots 0\rangle |00 \dots 0\rangle &\mapsto \sum_{i \in \{0,1\}^{l-1}} \alpha_{l,i} |i\rangle |r(s, i)\rangle |00 \dots 0\rangle \text{ (CBRNG)} \\
&\mapsto \sum_{i \in \{0,1\}^{l-1}} \alpha_{l,i} |i\rangle |r(s, i)\rangle |s_q(i)\rangle \text{ (sampling from } q_l(x)) \\
&\mapsto \sum_{i \in \{0,1\}^{l-1}} \alpha_{l,i} |i\rangle |00 \dots 0\rangle |s_q(i)\rangle \text{ (CBRNG)}
\end{aligned} \tag{4.32}$$

where in the last step we apply the inverse circuit of the quantized CBRNG.

The next step is determining whether  $s_q(i)$  should be accepted or rejected. We uniformly sample  $r_q(s', i)$  from  $[0, Q_l q_l(s_q(i))]$  using another CBRNG with seed  $s'$ :

$$\begin{aligned}
\sum_{i \in \{0,1\}^{l-1}} \alpha_i |i\rangle |s_q(i)\rangle |00 \dots 0\rangle |00 \dots 0\rangle &\mapsto \sum_{i \in \{0,1\}^{l-1}} \alpha_i |i\rangle |s_q(i)\rangle |r_q(s', i)\rangle |0\rangle \text{ (CBRNG)} \\
&\mapsto \sum_{i \in \{0,1\}^{l-1}} \alpha_i |i\rangle |s_q(i)\rangle |r_q(s', i)\rangle |r_q(s', i) \leq p_l(s_q(i))\rangle
\end{aligned} \tag{4.33}$$

Now, if  $r_q(s', i) \leq p_l(s_q(i))$ , then  $s_q(i)$  is accepted as  $\theta_i$ . Otherwise, we need to repeat the above process using another set of random numbers,  $r(s, i + j \cdot 2^n)$  and  $r_q(s', i + j \cdot 2^n)$  where  $j = 1$  for the second round, and  $j = k - 1$  for the  $k$ th round if necessary. For each round, we also need to use new ancilla registers to store  $r, s_q$ , and  $r_q$  values.

Finally, we compute how many times this rejection sampling process needs to be repeated for the  $l$ th qubit, which is denoted by  $N_l$ . We show in the following that if we need all  $\theta_i$  to be accepted with high probability after  $N_l$  rounds, it suffices to have  $N_l = \mathcal{O}(n)$ , a constant value independent of  $l$ . Since the probability for each sample to be accepted is  $p_{\text{suc},l} = \mathcal{O}(1)$ , the probability of being accepted after  $N_l$  rounds is  $1 - (1 - p_{\text{suc},l})^{N_l}$ . Therefore, if  $N_l = 2vn$  with  $v > 1$  being a constant satisfying  $(1 - p_{\text{suc},l})^v < 1/2$ , we can achieve  $(1 - p_{\text{suc},l})^{N_l} = ((1 - p_{\text{suc},l})^{2v})^n \ll 2^{-2n}$ . Now, one can use binomial approximation to show that the probability for all  $2^{l-1}$  values to be accepted is

$$(1 - (1 - p_{\text{suc},l})^{N_l})^{2^{l-1}} \approx 1 - 2^{l-1}(1 - p_{\text{suc},l})^{N_l} \geq 1 - 2^{l-1-2n} \geq 1 - \mathcal{O}(2^{-n}), \quad (4.34)$$

which is arbitrarily close to 1. Therefore, it suffices to apply  $\mathcal{O}(n)$  rounds of the above rejection sampling procedure for each binary data loader to generate all  $\theta_i$ s in superposition. This requires  $\mathcal{O}(n)$  random seeds for each  $l$ ,  $\mathcal{O}(n^2)$  random seeds in total, and the total number of rounds (or the circuit depth) is  $\mathcal{O}(n^2)$ . Since all random seeds are determined classically and loaded into the quantum circuit, all random numbers and  $r_q(s, i + j \cdot 2^n)$  values are generated deterministically, and all scratch qubits can be erased in the end. This concludes our initial state preparation algorithm based on rejection sampling.

## 4.2 Other initial state preparation

We also summarize some other initial states that may be interesting for actual protein dynamics simulation in other models than GNM.

**Deterministic initialization.** For instance, we may assume there is a perturbation on the displacement (or velocity) of the 1st atom, e.g.  $\mathbf{u}_1(0) = 1$  (or  $\dot{\mathbf{u}}_1(0) = 1$ ) and set the rest of amplitudes as 0. In this case, we can initiate the state as  $|\psi(0)\rangle = |0\rangle$ . In more general, we assume there is a delta-function  $\delta(t)$  acting on the system  $M \frac{d^2}{dt^2} \mathbf{u} + Z \frac{d}{dt} \mathbf{u} + H \mathbf{u} + \delta(t) = 0$ , giving certain initial displacement and velocity of certain atoms.

**Dynamics driven by steered forces.** One important implementation approach for molecular dynamics is the steered molecular dynamics (SMD) [61, 60], where one can start with an equilibrium configuration of the biomolecule, followed by a mechanical force applied to the end of the molecule,

$$M \frac{d^2}{dt^2} \mathbf{u} + H \mathbf{u} = f(t).$$

The goal is to stretch the system so that it will not be stuck in a local minimum. In this case, we can start with zero initial configuration for the displacement and velocity, and the problem is how to incorporate the time-dependent force  $f(t)$ .

**Initialization from a low-dimensional space.** The intuition is from the observation that the conformation changes occur in a low-dimensional space with low eigenvalues.

**Multiple inputs with uncertainty.** We can coherently simulate the protein dynamics once with multiple inputs with uncertainty  $|\psi(0, z)\rangle$  where  $z$  is a random variable with  $M$  samples, and compute the ensemble-averaged observables of the solution in terms of  $\xi$ . This admits a potential exponential speedup in terms of  $M$ . For Schrödinger-type equations, an uncertainty from Hamiltonians  $H$  (e.g. random media) can also be transformed into an uncertainty from the initial state. The quantum algorithms for uncertainty quantification refer to [52].

## 5 Matrix connectivity loading

In the previous work of simulating coupled oscillator systems [11], the spring settings are pre-defined and treated as the oracle  $F$ . The implementation of the oracle, however, could be a roadblock for end-to-end applications of this algorithm. Ideally, the oracle should be constructed efficiently to maintain the exponential speedup of simulation in both gate complexity and circuit depth, meaning that the data access oracle should perform only  $\text{polylog}(N)$  gates in  $\text{polylog}(N)$  depth. However, this is difficult due to Theorem 2.10, as the number of oscillators is  $\Omega(N)$ . Therefore, we mainly consider the circuit depth to ensure the exponential speedup in time complexity.

**Problem 3** (Low-depth matrix connectivity loading). *We need to build a data access oracle to load the matrix  $K$  onto the quantum algorithm in  $\mathcal{O}(\text{polylog } N)$  depth.*

Furthermore, since constructing a circuit to load  $K$  may take a significant amount of effort, it is preferable if a slightly different protein (with different atom positions, additional or removed residues, etc.) can be loaded by only changing a limited number of bits stored in the circuit. We also consider the complexity of modifying the protein.

**Problem 4** (Efficient modification of  $K$ ). *Suppose  $K$  is  $d$ -sparse, we need to build a data access oracle to load the matrix  $K$  onto the quantum algorithm in  $\mathcal{O}(\text{polylog } N)$  depth, and it supports efficient modification of the protein structure.*

We start by implementing an oracle of  $|i, j\rangle \mapsto |i, j\rangle |K_{i,j}\rangle$  for any  $i, j \in [N]$ . Although the number of  $(i, j)$  pairs is  $\mathcal{O}(N^2)$ , a realistic molecule usually has some sort of locality such that only  $\mathcal{O}(N)$  of  $K_{ij}$  are non-zero. For instance, as shown in Equation (A.9), the connection between any 2 residues in Gaussian network model (GNM) is determined by the cutoff radius. Similarly, for the anisotropic network model (ANM), the spring constants are determined by the distance between the nodes in three dimensions. However, in some other models such as HCA shown in Equation (A.13), interactions between any pair of constituent atoms are non-zero, so the number of non-zero terms in the  $F$  matrix is  $\mathcal{O}(N^2)$ .

Since in most models above, the spring constant of most oscillators between 2 atoms or residues, say  $i$  and  $j$ , is determined by the distance between them by an efficiently computable function

$K_{i,j} = f_K(|\vec{x}_i - \vec{x}_j|)$  where  $\vec{x}_i$  and  $\vec{x}_j$  are coordinates of the  $i$ th and the  $j$ th atoms, respectively. Therefore, it suffices for us to just load the coordinates of all atoms or residues and implement an oracle computing the  $f_K$  function.

### 5.1 Atom/residue position loading

Atom coordinates of the protein determine its molecular structure, which is usually studied by cryo-electron microscopy [102], or the fast-developing computational predictions based on large-scale neural networks [63], instead of being generated efficiently by a computer program. Therefore, those atomic-level data has high level of randomness and is difficult to compress with a ratio better than a constant value. In fact, even constant-ratio compression may ruin the scientific value of the molecular dynamics simulation, since exact coordinates of each atom must be loaded to fulfill the precision requirements of microscopic dynamics simulation. Hence, it is necessary to load all atomic position data into quantum memories to perform a sufficiently accurate molecular dynamics simulation of the given protein.

It is worth mentioning that a wild idea can be implementing a trained classical neural networks (such as AlphaFold) using quantum gates, such that the structure of the protein can be predicted using the quantum circuit, and there's no need to manually load the atom positions. However, this is difficult in the foreseeable future due to the astronomical size of those neural networks.

Loading classical data into a quantum system necessitates the usage of circuit-based QROM introduced in preliminaries (which has  $\mathcal{O}(\log N)$  circuit depth and requires  $\mathcal{O}(N \log N)$  gates), which enables an oracle for the coordinates of any constituent atom, i.e. a unitary  $U_x$  such that

$$U_x \sum_i \alpha_i |i\rangle |0, 0, 0\rangle = \sum_i \alpha_i |i\rangle |x_i, y_i, z_i\rangle. \quad (5.1)$$

The matrix element  $K_{i,j}$  between any pair of atoms  $i, j$  can finally be computed by calling the atomic position oracle twice and the spring constant function oracle  $U_f$ , yielding the matrix element loading oracle:

$$|i\rangle |j\rangle |\vec{0}\rangle |\vec{0}\rangle |0\rangle \xrightarrow{U_x \otimes U_x} |i\rangle |j\rangle |\vec{x}_i\rangle |\vec{x}_j\rangle |0\rangle \xrightarrow{U_f} |i\rangle |j\rangle |\vec{x}_i\rangle |\vec{x}_j\rangle |f_K(|\vec{x}_i - \vec{x}_j|)\rangle. \quad (5.2)$$

### 5.2 Brute-force sparse access

If we wish to use the simulation algorithm proposed in Ref. [11], the access model of the  $K$  matrix needs to be *sparse*, which means that for any  $i, k$ , the matrix loading oracle should give  $K_{i,j}$  where  $j$  is the  $k$ th non-zero element of the  $i$ th row of  $K$ . The sparse access is the requirement to employ many efficient digital quantum simulation algorithms for sparse Hamiltonians. The data access in this case consists of  $U_x$ ,  $U_f$ , and the *sparse oracle*  $U_s$  which is defined by

$$U_s |i\rangle |k\rangle |0\rangle = |i\rangle |k\rangle |j(i, k)\rangle \quad (5.3)$$

where  $j(i, k)$  is the  $k$ th non-zero element of the  $i$ th row of  $K$ . Once  $i$  and  $j$  are known, one can apply  $U_x$  and  $U_f$  to compute  $K_{i,j}$ . To implement  $U_s$ , one can compute  $j(i, k)$  classically for all  $i, k$

pairs, and then implement the coherent access to all  $(i, k) \mapsto j(i, k)$  by QROM. The total amount of data to be stored is  $\mathcal{O}(Nd)$  if  $K$  is  $d$ -sparse. We can thus claim that [Problem 3](#) is solved.

**Theorem 5.1.** *A sparse data access oracle to  $K$  can be implemented in  $\mathcal{O}(\log N)$  depth using  $\mathcal{O}(N \log(N))$  gates.*

We notice that due to the randomness in protein structure data, the naive algorithm for computing  $j(i, k)$  involves calling the protein structure database and calculating the distances between all pairs of atoms in the model, yielding a  $\mathcal{O}(N^2)$  amount of classical computation, and the information-theoretic lower bound is  $\Omega(Nd)$ . Moreover, modification of the sparse oracle is costly. For instance, consider an atom  $i'$  with position far away from all other atoms (i.e. it has no interaction with any other atom). If we decide to modify it so that it becomes within the reach of  $d$  other atoms, then we need to add  $\mathcal{O}(d)$  entries to  $j(i', k)$  and modify up to  $\mathcal{O}(d^2)$  entries of  $j(i, k)$  for other  $i$ 's, since we may need to change the order of non-zero elements in its row. The same cost also applies to *adding* or *removing* atoms from the protein molecule.

### 5.3 A flexible binary tree data structure from Ref. [\[66\]](#)

The brute-force sparse oracle construction suffers from a huge cost of modification, especially when  $d$  is large, and thus lacks flexibility. Moreover, in some configurations of GNM or ANM, especially when the cut-off radius is large, the matrix might not even be sparse. Therefore, in this subsection, we employ the data structure introduced in Ref. [\[66\]](#) to store each row of the Hamiltonian  $H$  using a binary tree, allowing for efficient quantum readout and classical modification of every row. This data structure is used in Ref. [\[100\]](#) to simulate the dynamics of dense Hamiltonians. Note that here we directly work on the Hamiltonian  $H$  as defined in Ref. [\[11\]](#) which contains information on both spring constants and masses of all elements.

Let  $T^i$  represent a binary tree storing the  $i$ th row of  $H$ , thus  $T := (T^1, T^2, \dots, T^N)$  stores the whole  $H$  matrix. Nodes of  $T^i$  are real or complex values, and they are indexed by a binary string  $s \in \{0, 1\}^1 \cup \{0, 1\}^2 \cup \dots \cup \{0, 1\}^n$  (recall that  $n = \log N$ ). The structure of  $T^i$  is defined as follows, where  $|\cdot|$  denotes the number of bits in the binary string.

- If  $|s| = n$ , then  $s$  corresponds to a leaf node. Its value satisfies  $T_s^i = H_{i,s}^*$ .
- If  $|s| < n$ , then  $s$  corresponds to a branch node, and its left-child node and right-child node are  $s0$  and  $s1$  respectively. Its value is real and satisfies  $T_s^i = |T_{s0}^i| + |T_{s1}^i|$ .

In other words, each branch node of  $T^i$  represents the sum of  $|H_{i,j}|$  for a specific range of  $j$ . If we construct the QROM access to elements of every  $T^i$  binary tree, then we can employ the algorithm of Refs. [\[66, 100\]](#) to produce a quantum state that is proportional to the  $i$ th row of the matrix with high probability:

$$|i\rangle |0\rangle^{\otimes n} \rightarrow |i\rangle \sum_{j=0}^{N-1} \sqrt{H_{i,j}^*} |j\rangle \quad (5.4)$$

using a  $\mathcal{O}(n^2)$  depth quantum circuit.

Recall in Ref. [11],  $H$  is defined as

$$H = - \begin{pmatrix} 0 & B \\ B^\dagger & 0 \end{pmatrix} \quad (5.5)$$

and  $B$  satisfies

$$\begin{aligned} \sqrt{MB} |j, j\rangle &= \sqrt{\kappa_{jj}} |j\rangle \\ \sqrt{MB} |j, k\rangle &= \sqrt{\kappa_{jk}} (|j\rangle - |k\rangle) \end{aligned} \quad (5.6)$$

Therefore, the matrix  $B$  stores a similar amount of information as the  $K$  matrix, except that the inverse mass of each spring is multiplied by the spring coefficients.

We claim that the binary-tree data structure for  $H$  above supports the following efficient modifications of the protein structure. Here focus on *engineering complexity*, which is defined as the number of values stored in QROM to be modified, since constructing a hard-coded QROM is an expensive engineering effort. Note that according to Refs. [66, 100], modification of each matrix element has  $\text{polylog}(N)$  engineering complexity. Hence we only consider the number of matrix elements to be modified in the following discussions.

1. Mass modification. If the mass of a single element of the system needs to be modified, then a total number of  $\mathcal{O}(d)$  matrix elements need to be modified.
2. Position modification. If the position of one element is changed, then all spring constants connecting to it need to be changed, which is also  $\mathcal{O}(d)$ .
3. Add an element. First, there needs to be a new row of  $B$ , thus a new binary tree  $T^{N+1}$  to store the row.  $T^{N+1}$  has  $\mathcal{O}(d)$  non-zero leaf nodes, thus the number of leaf node modifications is  $\mathcal{O}(d)$ . Second, every row that has connection to the new node should have a new leaf node, which is also  $\mathcal{O}(d)$ . The total number of modifications is  $\mathcal{O}(d)$ .
4. Remove an element. First, the tree  $T^i$  needs to be deleted, where  $i$  is the index of the element. For every other tree that has a connection with the  $i$ th element, one leaf node needs to be removed, which leads to an overall number of leaf node modifications  $\mathcal{O}(d)$ . Note that in such a process, what we are essentially doing is to remove all springs connecting the  $i$ th element and the others. Therefore, when preparing the initial state, one can still assign position and velocity for the element, and both values will not change during the process of simulation, thus making no contribution to the dynamics of the system.

With this, we conclude that **Problem 4** is also solved.

**Theorem 5.2.** *There is a data access oracle of  $K$  in  $\mathcal{O}(\text{polylog } N)$  depth supporting modification of any element of the protein structure by changing  $\mathcal{O}(d \cdot \text{polylog } N)$  values stored in QROM.*



## 6 Simulating protein dynamics on quantum computers

In this section, we consider quantum algorithms for simulating protein dynamics with non-Hermitian structures and external forces or noises. For the standard harmonic approximation model, we perform Hamiltonian simulation to propagate initial state  $|\psi(0)\rangle$  to a target final state  $|\psi(T)\rangle$ , which includes information on the motions of proteins. For general non-Hermitian dynamics, we consider quantum linear ODE solvers or Linear Combination of Hamiltonian Simulations (LCHS) to produce the final states or the Feymann-Kac history states (known as the dense output [83]). For Langevin dynamics, we apply open quantum system simulations to produce the final states described by the density matrix.

As introduced in Section 3, we are interested in the harmonic approximation model near by an equilibrium as in (3.2)

$$m_i \ddot{u}_i = - \sum_{j=1}^N K_{ij} u_j, \quad (6.1)$$

and the harmonic approximation model away from an equilibrium as in (3.6)

$$m_i \ddot{u}_i = - \sum_{j=1}^N K_{ij} u_j + F_i. \quad (6.2)$$

We can apply the Hamiltonian simulation algorithm to produce the final state of the former model. We need to apply quantum linear ODE solvers to simulate the later model, or to produce the history state of the former model.

### 6.1 Hamiltonian Simulation

Our goal is to develop a quantum algorithm to efficiently simulate protein dynamics. In our problem formulation, the input and output are quantum states whose amplitudes encode the velocities and displacements of the protein molecules. Inspired by [11], we consider the Hamiltonian simulation algorithm for protein dynamics, modeled by the equation of motions. We reproduce the harmonic oscillator system in (3.2) as

$$M \frac{d^2 \mathbf{u}(t)}{dt^2} + K \mathbf{u}(t) = 0. \quad (6.3)$$

We consider a change of variables

$$\mathbf{y}(t) = \sqrt{M} \mathbf{u}(t), \quad (6.4)$$

where  $\sqrt{M}$  is a matrix square root, which is a trivial operation since  $M$  is diagonal. This allows us to eliminate  $M$  from the equation and rewrite the dynamics as

$$\ddot{\mathbf{y}}(t) + A \mathbf{y}(t) = 0, \quad (6.5)$$

where  $A := (\sqrt{M})^{-1} K (\sqrt{M})^{-1}$ . The key observation is that any solution  $\mathbf{y}(t)$  of (6.5) should also satisfy

$$\ddot{\mathbf{y}}(t) + i\sqrt{A}\dot{\mathbf{y}}(t) = i\sqrt{A}\left(\dot{\mathbf{y}}(t) + \sqrt{A}\mathbf{y}(t)\right), \quad (6.6)$$

hence its solution is given by

$$\dot{\mathbf{y}}(t) + \sqrt{A}\mathbf{y}(t) = e^{i\sqrt{A}t} \left( \dot{\mathbf{y}}(0) + \sqrt{A}\mathbf{y}(0) \right). \quad (6.7)$$

As a result, the solution at time  $t$  can be obtained by simulating  $e^{i\sqrt{A}t}$  via a Hamiltonian simulation algorithm. More specifically, suppose that we have access to  $A$  rather than  $\sqrt{A}$ . Following the incidence matrix approach [36, 11], we aim to construct a matrix  $B$  such that  $BB^\dagger = A$  and a block Hamiltonian

$$H = - \begin{bmatrix} 0 & B \\ B^\dagger & 0 \end{bmatrix}. \quad (6.8)$$

We notice that the first block of  $H^2$  is  $A$ . We turn to simulate the Schrödinger equation

$$i \frac{d}{dt} |\psi(t)\rangle = H |\psi(t)\rangle. \quad (6.9)$$

with

$$|\psi(t)\rangle := \frac{1}{\sqrt{2E}} [\dot{\mathbf{y}}(t), iB^\dagger \mathbf{y}(t)]^T. \quad (6.10)$$

On natural choice of  $B$  is  $-\sqrt{A}$ . But the choice is clearly not unique. In particular, one can pick a rectangular matrix to fulfill the condition  $BB^\dagger = A$ . We follow the choice in [11], where

$$\sqrt{M}B|j, k\rangle = \begin{cases} \sqrt{K_{jk}}(|j\rangle - |k\rangle), & j < k \\ \sqrt{K_{jj}}|j\rangle, & i = j. \end{cases} \quad (6.11)$$

This choice satisfies  $\sqrt{M}B(\sqrt{M}B)^\dagger = K$  and hence  $BB^\dagger = A$ . So we can block encode  $\sqrt{M}B$  and then divide it by  $\sqrt{M}^{-1}$  to obtain  $B$ .

**Problem 5.** We consider the harmonic oscillator system (6.3) and reshape it as (6.5). Let  $M$  be an  $N \times N$  diagonal matrix with positive diagonal elements, and  $K$  be an  $N \times N$  real symmetric, positive-definite, and  $d$ -sparse matrix. Define the normalized state

$$|\psi(t)\rangle := \frac{1}{\sqrt{2E}} [\dot{\mathbf{y}}(t), iB^\dagger \mathbf{y}(t)]^T, \quad (6.12)$$

where  $E > 0$  is a normalizing constant. Assume we have unitaries  $U_M$  and  $U_F$  that prepare  $M$  and  $K$ , and a unitary  $U_I$  that prepares the initial state  $|\psi(0)\rangle$ . Given  $T > 0$ , the goal is to produce  $|\psi(T)\rangle$  within  $\ell_2$  error tolerance  $\epsilon$ .

Here we are interested in producing the state  $|\psi(t)\rangle$  at a certain time  $t$ . This state encodes the velocities ( $\dot{\mathbf{y}}(t)$ ) and displacements ( $\mathbf{y}(t)$ ) of the protein molecules, hence it can be used to estimate the kinetic or potential energies.

The state-of-the-art Hamiltonian simulation algorithm can propagate  $e^{iHt}$  with  $\mathcal{O}(\|H\|t + \log(1/\epsilon))$  queries to the oracles of  $H$  [85]. Based on the discussion above, especially Eqs. (6.8) and (6.11), a direct estimate is as follows:  $\|H\| = \sqrt{\kappa_A}$ ,  $\kappa_A = K_{\max}/m_{\min}$  with  $m_{\max} \geq m_j \geq m_{\min} > 0$ , and  $K_{\max} \geq K_{jk}$ . We reproduce the complexity of Hamiltonian simulation algorithm [11] as below.

**Theorem 6.1** (Theorem 1 of [11]). *Problem 5 can be solved with a quantum algorithm that makes*

$$\mathcal{O}\left(\sqrt{\kappa_A}T + \log(1/\epsilon)\right) \quad (6.13)$$

*queries to the unitaries  $U_M$  and  $U_F$  that prepare  $M$  and  $F$ , respectively, and one query to the unitary  $U_I$  that prepares  $\mathbf{x}(0)$ , where  $\kappa_A = K_{\max}/m_{\min}$ ,  $m_{\max} \geq m_j \geq m_{\min} > 0$ , and  $K_{\max} \geq K_{jk}$ . The one- or two-qubit gate complexity is larger by a poly-logarithmic factor.*

## 6.2 LCHS Method for steered protein dynamics

We now consider the normal mode dynamics under a mechanical force (3.6). We reproduce it as

$$M \frac{d^2 \mathbf{u}(t)}{dt^2} + K \mathbf{u}(t) = F. \quad (6.14)$$

We consider a change of variables

$$\mathbf{y}(t) = \sqrt{M} \mathbf{u}(t), \quad (6.15)$$

that allows us to rewrite the dynamics as

$$\ddot{\mathbf{y}}(t) + A \mathbf{y}(t) = \mathbf{b}, \quad (6.16)$$

where  $A := (\sqrt{M})^{-1} K (\sqrt{M})^{-1}$  and  $\mathbf{b} := M^{-1} F$ . Any solution  $y(t)$  satisfies

$$\ddot{y}(t) + i\sqrt{A}\dot{y}(t) = i\sqrt{A}\left(\dot{y}(t) + \sqrt{A}y(t)\right) + \mathbf{b}, \quad (6.17)$$

hence its solution is

$$\dot{y}(t) + \sqrt{A}y(t) = e^{i\sqrt{A}t} \left( \dot{y}(0) + \sqrt{A}y(0) \right) + \int_0^t e^{i\sqrt{A}(t-s)} \mathbf{b}(t-s) ds. \quad (6.18)$$

This is a non-unitary dynamics and can be viewed as linear combination of Hamiltonian simulation.

Similarly, we cannot have access to  $\sqrt{A}$ , so we aim to construct a matrix  $B$  such that  $BB^\dagger = A$  and a block Hamiltonian

$$H = - \begin{bmatrix} 0 & B \\ B^\dagger & 0 \end{bmatrix}. \quad (6.19)$$

We notice that the first block of  $H^2$  is  $A$ . We turn to simulate the system of linear ODEs

$$\frac{d}{dt} |\psi(t)\rangle = -iH |\psi(t)\rangle + |\bar{b}\rangle. \quad (6.20)$$

with

$$|\psi(t)\rangle := \frac{1}{\sqrt{2E}} [\dot{\mathbf{y}}(t), iB^\dagger \mathbf{y}(t)]^T. \quad (6.21)$$

and

$$|\bar{b}\rangle := [\mathbf{b}(t), 0]^T. \quad (6.22)$$

We describe the problem as follows.

**Problem 6.** We consider the inhomogeneous harmonic oscillator system (6.14). Under the same assumption of Problem 5, the goal is to produce  $|\psi(T)\rangle$  within  $\ell_2$  error tolerance  $\epsilon$ .

Due to the inhomogeneous term in the differential equation, we cannot directly apply the standard Hamiltonian simulation in Theorem 6.1. Instead, we can apply the Theorem 6.3 to the final state problem or the history state problem.

We can also apply the Linear Combination of Hamiltonian Simulation (LCHS) to produce the final state with near-optimal dependence on all parameters [5, 3]. Compared to the Quantum Linear ODE Solver in Theorem 6.3, the LCHS method can significantly reduce the state preparation cost.

**Theorem 6.2** (Theorem 2 of [3]). *Problem 6 can be solved with a quantum algorithm that makes*

$$\mathcal{O}\left(q\sqrt{\kappa_A}T \log^{1+1/\beta}\left(\frac{1}{\epsilon}\right)\right) \quad (6.23)$$

queries to the unitaries  $U_M$  and  $U_F$  that prepare  $M$  and  $F$ , and  $\mathcal{O}(q)$  queries to the unitaries  $U_I$  and  $U_b$  that prepare  $\mathbf{x}(0)$  and  $\mathbf{b}(t)$ , where  $\kappa_A = K_{\max}/m_{\min}$ ,  $m_{\max} \geq m_j \geq m_{\min} > 0$ ,  $K_{\max} \geq K_{jk}$ ,  $q = \frac{\|\mathbf{x}_0\| + \|\mathbf{b}\|_{L^1}}{\|\mathbf{x}(T)\|}$ , and  $\|\mathbf{b}\|_{L^1} = \int_0^T \mathbf{b}(s)ds$ ,  $\beta \in (0, 1)$ . The one- or two-qubit gate complexity is larger by a poly-logarithmic factor.

In our case, we have Hermitian matrix  $A(t) = H(t)$ .

### 6.3 Quantum Linear ODE Solver for the dense outputs

We next consider the target of producing the history state of the protein dynamics. The general non-unitary process requires the usage of the quantum linear ODE solver. We again consider the general inhomogeneous ODE system (6.14)

$$M \frac{d^2 \mathbf{u}(t)}{dt^2} + K \mathbf{u}(t) = F. \quad (6.24)$$

Given an initial condition  $|\psi(t)\rangle$ , we divide the time interval  $[0, T]$  into  $N_t = \mathcal{O}(T \log(1/\epsilon))$  sub-intervals, with  $0 = t_0 < t_1 < \dots < t_{N_t} = T$ ,  $h_k = t_{k+1} - t_k$ , where the nodes  $\{t_k\}$  can be constructed by certain quadrature rules. For a time-independent Hamiltonian  $H$ , we construct  $(N_t + 1)n \times (N_t + 1)n$  linear system

$$L|\Psi\rangle = |B\rangle \quad (6.25)$$

as the form

$$\begin{pmatrix} I & & & & & \\ -iHh & I & & & & \\ & & \ddots & \ddots & & \\ & & & & -iHh & I \\ & & & & & -iHh & I \end{pmatrix} \begin{pmatrix} \psi(t_0) \\ \psi(t_1) \\ \vdots \\ \psi(t_{N_t-1}) \\ \psi(t_{N_t}) \end{pmatrix} = \begin{pmatrix} |\psi(0)\rangle \\ 0 \\ \vdots \\ 0 \\ 0 \end{pmatrix}. \quad (6.26)$$

We can perform the quantum linear ODE solvers such as [21, Theorem 2] to produce the history state

$$|\Psi\rangle = \frac{1}{\sqrt{N_t + 1}} \sum_{k=0}^{N_t} |k\rangle |\psi(t_k)\rangle \quad (6.27)$$

with query and gate complexity

$$\mathcal{O}(Q) \quad (6.28)$$

as defined in [Theorem 6.1](#). Here we use the fact that the rescaling factor of the Hamiltonian dynamic satisfies  $g = \frac{\max_{t \in [0, T]} \|\Psi(t)\|}{\|\Psi(T)\|} = 1$ , so there are no additional factors.

The quantum linear ODE solver requires  $\mathcal{O}(Q)$  copies of the input states  $|\psi(0)\rangle$  in the linear system (6.25), while the Hamiltonian simulation algorithm only requires a single copy of  $|\psi(0)\rangle$ . We state the results as below.

**Problem 7.** *We consider the harmonic oscillator system (6.3) or (6.14). Under the same assumption of [Problem 6](#), and given certain quadrature nodes  $0 = t_0 < t_1 < \dots < t_{N_t} = T$ , the goal is to produce the history state*

$$|\Psi\rangle = \frac{1}{\sqrt{N_t + 1}} \sum_{k=0}^{N_t} |k\rangle |\psi(t_k)\rangle, \quad (6.29)$$

within  $\ell_2$  error tolerance  $\epsilon$ .

**Theorem 6.3.** *[Problem 7](#) can be solved with a quantum algorithm that makes*

$$\mathcal{O}\left(q\sqrt{\kappa_A}T \text{polylog}(1/\epsilon)\right) \quad (6.30)$$

queries to the unitaries  $U_M$  and  $U_F$  that prepare  $M$  and  $F$ , and the unitaries  $U_I$  and  $U_b$  that prepare  $\mathbf{x}(0)$  and  $\mathbf{b}(t)$ , where  $\kappa_A = \frac{K_{\max}}{m_{\min}}$ ,  $m_{\min} \geq m_j \geq m_{\min} > 0$ , and  $K_{\max} \geq K_{jk}$ ,  $q = \frac{\|\mathbf{x}_0\| + \|\mathbf{b}\|_{L^1}}{\|\mathbf{x}(T)\|}$ , and  $\|\mathbf{b}\|_{L^1} = \int_0^T \mathbf{b}(s) ds$ . The one- or two-qubit gate complexity is larger by a poly-logarithmic factor.

## 6.4 Quantum algorithms for simulating Langevin dynamics

For molecular dynamics with stochastic effects, we consider the Langevin dynamics (3.3) as the problem model

$$M \frac{d^2 \mathbf{u}}{dt^2} + \gamma \frac{d\mathbf{u}}{dt} + K\mathbf{u} + \sigma \xi(t) = 0. \quad (6.31)$$

Here  $\gamma > 0$  is the friction coefficient from the interaction of the protein with the surrounding solvent. In addition,  $\xi(t)$  is a white noise with independent entries acting on each velocity component. The noise amplitude is related to the damping coefficient according to the fluctuation-dissipation theorem,

$$\sigma = \sqrt{2k_B T \gamma}.$$

To formulate an efficient quantum algorithm for (6.31), we first show that the Langevin equation (6.31) can be converted into a stochastic Schrödinger equation. Again motivated by [36], we

introduce variable  $\mathbf{v}(t)$ , and consider the following dynamics,

$$\frac{d}{dt} \begin{bmatrix} \mathbf{u} \\ \mathbf{v} \end{bmatrix} = -i \begin{bmatrix} 0 & B \\ B^\dagger & 0 \end{bmatrix} \begin{bmatrix} \mathbf{u} \\ \mathbf{v} \end{bmatrix} - \begin{bmatrix} 0 & 0 \\ 0 & \gamma I \end{bmatrix} \begin{bmatrix} \mathbf{u} \\ \mathbf{v} \end{bmatrix} + \begin{bmatrix} 0 \\ \sigma I \end{bmatrix} \xi(t) \quad (6.32)$$

By differentiating the first equation, followed by a substitution of the second equation, we obtain the Langevin dynamics,

$$\frac{d^2}{dt^2} \mathbf{u} = -BB^\dagger \mathbf{u} - \gamma \frac{d}{dt} \mathbf{u} + \sigma \xi(t). \quad (6.33)$$

Therefore, by choosing  $B$ , such that  $K = BB^\dagger$ , we can map the Langevin equation (6.31) to a stochastic Schrödinger equation. However, it is interesting to note that, unlike the stochastic Schrödinger equation from the theory of open quantum systems [26], this equation has an additive noise, instead of a multiplicative noise.

We will express (6.32) as a stochastic differential equation in the Itô's form,

$$\frac{d}{dt} |\phi\rangle = -(iH + \gamma I) |\phi\rangle + \Sigma \xi(t). \quad (6.34)$$

Here  $H$  is defined as (6.19) with  $\|H\| = \sqrt{\kappa_A}$ , and  $\Sigma$  is a matrix with the property that

$$\Sigma \Sigma^T = \begin{bmatrix} 0 & 0 \\ 0 & \sigma^2 I \end{bmatrix}. \quad (6.35)$$

Define an operator  $\rho(t) := \mathbb{E}[|\phi(t)\rangle\langle\phi(t)|]$ . Then the Itô Lemma implies that  $\rho$  solves the following master equation,

$$\frac{d}{dt} \rho = -i[H, \rho] - \{\gamma I, \rho\} + \Sigma \Sigma^\dagger, \quad (6.36)$$

where  $\gamma < 0$ .

In the Langevin dynamics model, we are interested in solving the following problem.

**Problem 8.** *We consider the Langevin dynamics (6.36). Under the same assumption of Problem 5, the goal is to produce  $\rho$  within  $\ell_2$  error tolerance  $\epsilon$ .*

**Theorem 6.4.** *Problem 8 can be solved using*

$$\mathcal{O}\left(\sqrt{\kappa_A T} + \log(1/\epsilon)\right) \quad (6.37)$$

*queries to unitaries  $U_M$  and  $U_F$  that prepare  $M$  and  $F$  and the unitaries  $U_I$  for  $\rho(0)$  and  $\xi(t)$ . The one- or two-qubit gate complexity is larger by a poly-logarithmic factor.*

*Proof.* Defined  $J = -iH - \gamma I$ . Then at each step, the density operator can be updated as follows,

$$\rho(t) = e^{tJ} \rho(0) e^{tJ^\dagger} + \int_0^t e^{\tau J} \Sigma \Sigma^\dagger e^{\tau J^\dagger} d\tau. \quad (6.38)$$

The first term is dissipative, due to  $\gamma > 0$ . The second term leads to a growth of  $\rho$ . We expect that as  $t \rightarrow \infty$ ,  $\rho(t) \propto (BB^\dagger)^{-1}$ . So it will not blow up.

In Eq. (6.38), the trace of the first term can be bounded as

$$\mathrm{Tr}(e^{jT} \rho(0) e^{tJ^\dagger}) = \mathrm{Tr}(\rho(0) e^{t(J^\dagger + J)}) = \mathrm{Tr}(\rho(0) e^{-2\gamma t I}) = e^{-2\gamma t} \mathrm{Tr}(\rho(0)) = \Theta(2^n e^{-2\gamma t}), \quad (6.39)$$

where we have assumed that we can prepare the initial state  $\rho(0)$  such that its initial variance is some constant, meaning that  $\mathrm{Tr}(\rho(0)) = \Theta(2^n)$ . To bound the trace of the second term, observe that  $\mathrm{Tr}(\Sigma \Sigma^\dagger) = \delta^2 \dim(B) = 2^n \sigma^2$ . We have

$$\mathrm{Tr} \left( \int_0^t e^{\tau J} \Sigma \Sigma^\dagger e^{\tau J^\dagger} d\tau \right) = \int_0^t d\tau \mathrm{Tr} \left( e^{jJ\tau} \Sigma \Sigma^\dagger e^{jJ^\dagger\tau} \right) \quad (6.40)$$

$$= \int_0^t d\tau \mathrm{Tr} \left( \Sigma \Sigma^\dagger e^{-2j\gamma I\tau} \right) \quad (6.41)$$

$$= \frac{1 - e^{-2\gamma t}}{2\gamma} \mathrm{Tr} \left( \Sigma \Sigma^\dagger \right) \quad (6.42)$$

$$= \frac{1 - e^{-2\gamma t}}{2\gamma} 2^n \sigma^2. \quad (6.43)$$

Since the two terms in Eq. (6.38) are not trace-preserving, we simulate the evolution by drawing a random sample according to the traces of the two terms and then performing the simulation of either of the terms according to the sampling outcome.

Because of Eqs. (6.39) and (6.43), the traces are easy to estimate. To prepare the state in Eq. (6.38), we first sample from the probability distribution proportional to the traces of the two terms, and then we either prepare the first or the second term depending on the sample outcome.

To implement the quantum completely positive map  $e^{tJ} \cdot e^{tJ^\dagger}$ , it suffices to implement the Kraus operator  $e^{tJ}$ . It is important to note that the operator  $e^{tJ}$  is essentially a scaled Hamiltonian evolution because  $e^{tJ} = e^{t(-iH - \gamma I)} = e^{-\gamma t} e^{-iHt}$ . Using the state-of-the-art Hamiltonian simulation algorithm [85], this complete positive map can be implemented with cost  $(\alpha t, +\mathrm{polylog}(1/\epsilon))$ , where  $\alpha$  is the normalizing constant of the block-encoding of  $H$ , which is upper bounded by  $\sqrt{\kappa_A}$ . The second term in Eq. (6.38), i.e.,  $\int_0^t e^{\tau J} \Sigma \Sigma^\dagger e^{\tau J^\dagger} d\tau$ , can be prepared in a similar way: we just randomly sample a  $\tau \in [0, t]$  and then implement the completely positive map  $e^{\tau J} \cdot e^{\tau J^\dagger}$  on initial state  $\Sigma \Sigma^\dagger$ . Finally, to prepare the initial state  $\Sigma \Sigma^\dagger$ , we just use two registers, where the first holds  $|1\rangle\langle 1|$  and the second holds a maximally mixed state.  $\square$

Given an observable  $O$ , we have the following result for estimating the expectation value  $\mathrm{Tr}(O\rho)$ .

**Theorem 6.5.** *Let  $O$  be an observable whose block-encoding has normalizing constant  $\beta$  and construction cost  $Q$ . For every  $\epsilon, \delta > 0$ , there exists a quantum algorithm that produces an estimate  $\xi$  of  $\mathrm{Tr}(\rho O)$  such that*

$$|\xi - \mathrm{Tr}(\rho O)| \leq \epsilon$$

*with probability at least  $1 - \delta$ . This algorithm uses each of the unitaries  $U_M$  and  $U_F$  that prepare  $M$  and  $F$ , the unitaries  $U_I$  for  $\rho(0)$  and  $\xi(t)$ , and the block-encoding  $Q$  of  $O$  a number of  $\mathcal{O}(\frac{\beta}{\epsilon} \log(1/\delta))$  times.*

*Proof.* To use Lemma 2.9, we need to implement a purification of  $\rho(T)$ . Note that Theorem 6.4 actually produces an ensemble instead of a purification. To create a purification, we use an additional register to coherently prepare the probability distribution. Since the probability distributions as in the proof of Theorem 6.4 are integrable, this superposition can be efficiently created by [53]. Then it is straightforward to use the algorithm in Theorem 6.4 controlled by this additional register to prepare a purification of  $\rho(T)$ . It suffices to use precision  $\epsilon$  in this step. Then use Lemma 2.9 and the statement follows.  $\square$

## 7 Computing properties of proteins

As in classical simulations, the goal of our quantum algorithms is to compute certain properties of proteins within a given error tolerance  $\epsilon$ . We consider a Hamiltonian system to represent the protein system with Hamiltonian  $H$ . In our paper, we consider two types of input models:

- (a) block encoding (BE) model: let  $U$  be an  $\alpha$ -block-encoding of the Hamiltonian  $H$ ;
- (b) Quantum evolution (QE) model: there is a quantum algorithm  $U(t)$  that prepares an amplitude-encoded solution  $|\psi(t)\rangle$  at time  $t$ .

We consider properties that can be expressed through an observable  $O$ . We let  $V$  be an  $\beta$ -block-encoding of the observable  $O$ .

The quantum evolution (QE) model is inspired by the Hamiltonian evolution model [43], where we have the explicit operator  $U = e^{iHt}$ . The QE models contain the quantum simulation of the homogeneous harmonic oscillator system (Problem 5), and the QE model can also include other dynamical models, such as the inhomogeneous oscillator system (Problem 6), history-state model (Problem 7), and Langevin dynamical system (Problem 8).

We discuss various types of application models with queries to the input model of  $H$  and  $O$  in the following sections.

### 7.1 Kinetic and potential energy

Inspired by [81, 11, 83], we first estimate the kinetic and potential energy of protein molecules.

**Theorem 7.1** (Theorem 5,6 of [11]). *Given a unitary  $U_D$  for a subset of molecules  $D \subset [n]$ , s.t.  $U_D|j\rangle = -|j\rangle$  for  $j \in D$  and  $U_D|j\rangle = |j\rangle$  for  $j \notin D$ . Let  $E$  be the total energy, which is conserved in time,  $K_D(t) = \frac{1}{2} \sum_{j \in V} m_j \dot{x}_j^2(t)$  be the kinetic energy, and  $P_D(t) = \frac{1}{2} \sum_{(j,j) \in V} \kappa_{jj} x_j^2(t) + \frac{1}{2} \sum_{(j,k) \in V} \kappa_{jk} (x_j(t) - x_k(t))^2$  be the potential energy. Then*

(i) *a quantum algorithm can produce  $\hat{k}_D(t)$  such that*

$$\left| \hat{k}_D(t) - K_D(t)/E \right| < \epsilon \quad (7.1)$$

*with probability  $1-\delta$ , which makes  $\mathcal{O}\left(\frac{\log(1/\delta)}{\epsilon}\right)$  queries of  $U_D$  and Hamiltonian simulation algorithm  $U(t)$  that prepares  $|\psi(t)\rangle$  in Theorem 6.1.*

(ii) *a quantum algorithm can produce  $\hat{p}_D(t)$  such that*

$$\left| \hat{p}_D(t) - P_D(t)/E \right| < \epsilon, \quad (7.2)$$



with probability  $1 - \delta$ , which makes  $\mathcal{O}\left(\frac{\log(1/\delta)}{\epsilon}\right)$  queries of  $U_D$  and Hamiltonian simulation algorithm  $U(t)$  that prepares  $|\psi(t)\rangle$  in [Theorem 6.1](#).

Similar as Proof of Theorem 5 of [\[11\]](#), we note that  $K_D(t)/E = \langle \psi(t) | \mathcal{P} | \psi(t) \rangle$  with projection  $\mathcal{P} = (I - U_D)/2$ . We can use amplitude estimation to estimate  $\langle \psi(t) | U_D | \psi(t) \rangle$  within  $2\epsilon$  and success probability  $1 - \delta$  with  $\mathcal{O}\left(\frac{\log(1/\delta)}{\epsilon}\right)$  use of  $U_D$  and copies of  $|\psi(t)\rangle$ , which is produced by  $U(t)$ .

We are also interested in producing dense outputs (time-accumulated observables) from the protein dynamics [\[81, 83\]](#). For the general quantum dense output problem with its early fault-tolerant quantum algorithm and nearly optimal time quantum algorithm, we refer to Problem 1 and Table 1 of [\[83\]](#).

As a certain type of dense output, we consider the time-accumulated kinetic energy of protein molecules, denoted as  $K_V$ . This quantity is closely related to time series analysis and spectral analysis of molecular dynamics, and it is of importance in understanding the effects of molecular aggregates and polymers. We follow the procedure in Section 6 of [\[81\]](#): given the total energy  $E_T = ET$  and discrete time subinterval  $\mathcal{D}_T = \{t_0 = 0, t_1, \dots, t_{K-1}, t_K = T\}$ , the ratio of kinetic energy  $K_V/E_T = \langle \psi | \mathcal{O} | \psi \rangle$  associates with the observable  $\mathcal{O}$  related to  $\mathcal{D}_T$  and the history state  $|\psi\rangle = \frac{1}{\sqrt{K+1}} \sum_{k=0}^K |k\rangle |\psi(t_k)\rangle$ .

**Theorem 7.2.** *Given a unitary  $U_D$  for subset of molecules and time  $D \subset [n] \times \mathcal{D}_T$ ,  $\mathcal{D}_T = \{t_0 = 0, t_1, \dots, t_{K-1}, t_K = T\}$ , s.t.  $U_D|j, k\rangle = -|j, k\rangle$  for  $(j, k) \in D$  and  $U_D|j, k\rangle = |j, k\rangle$  for  $(j, k) \notin D$ . Let  $E_T = ET$ ,  $E$  be the total energy preserved in time, and  $K_V = \frac{1}{2} \sum_{(j,k) \in V} m_j \dot{x}_j^2(t_k)$  be the time-accumulated kinetic energy. Then a quantum algorithm can produce  $\hat{k}_V$  such that*

$$|\hat{k}_V - K_V/E_T| < \epsilon \tag{7.3}$$

with probability  $1 - \delta$ , which makes  $\mathcal{O}\left(\frac{\log(1/\delta)}{\epsilon}\right)$  queries of  $U_D$  and quantum linear ODE solver  $U(t)$  that prepares the history state  $|\psi\rangle = \frac{1}{\sqrt{K+1}} \sum_{k=0}^K |k\rangle |\psi(t_k)\rangle$  in [Theorem 6.3](#).

## 7.2 Low vibration modes

In the context of protein dynamics, the eigenvector of the lowest nonzero eigenvalue are often associated with the structural changes, and more importantly, the protein functions [\[14\]](#). The main observation is that atomic displacements along high-frequency modes are energetically less favorable than those of equal magnitude along low-frequency modes.

Due to the translation symmetry, the stiffness matrix has a trivial null space. For example, the matrix that determines the vibration modes (e.g., see Eq. [\(A.9\)](#)) has one zero eigenvalue with eigenvector,  $N^{-1/2}(1, 1, \dots, 1)$ . Similarly the matrix (e.g., [\(A.12\)](#)) has three zero eigenvalues with zero eigenvectors,

$$N^{-1/2}(1, 0, 0, 1, 0, 0, \dots, 1, 0, 0), N^{-1/2}(0, 1, 0, 0, 1, 0, \dots, 0, 1, 0), N^{-1/2}(0, 0, 1, 0, 0, 1, \dots, 0, 0, 1).$$

Similarly, rotational invariance induces another three-dimensional null space. We denote the null space (or eigenspace with the 6 zero eigenvalues) by  $Y$ . Therefore, according to the Courant-Fischer

Theorem, the problem of finding the lowest normal mode can be formulated as follows,

$$\min_{\mathbf{v} \in Y^\perp} \frac{\mathbf{v}^T H \mathbf{v}}{\mathbf{v}^T \mathbf{v}} = \min_{|\psi\rangle \in Y^\perp} \langle \psi | H | \psi \rangle. \quad (7.4)$$

For this purpose of estimating low modes, we need a unitary

$$U(t) = \exp(-itH),$$

and an initial state  $|\psi_0\rangle$  that has enough overlap with  $|\psi\rangle$ .

Given known zero eigenspace  $Y$  and nonzero spectral gap  $\Delta$ , we construct a projector  $P_{Y^\perp} = I - \sum_{\mathbf{v} \in Y^\perp} \mathbf{v} \mathbf{v}^T$  onto nonzero eigenspace  $Y^\perp$ . Given initial state  $|\psi_0\rangle$  that has overlap with  $|\psi\rangle$  as  $p_0 = |\langle \psi_0 | \psi \rangle|^2$ , if there is a  $(\alpha, a, \epsilon)$ -block-encoding of  $H$ , we can perform quantum eigenstate filtering to estimate the (nonzero) ground state with cost  $\mathcal{O}(\alpha/(\Delta\sqrt{p_0}\epsilon))$  [76, Theorem 6].

To ensure that the initial state  $|\psi_0\rangle$  has sufficient overlap with  $|\psi\rangle$ , we may select a vector  $|\psi_0\rangle$  from a subspace generated from rotation-translation blocks (RTB) [45]. Such a subspace consists of atomic configurations where the atoms within each residue follow a rigid body rotation and translation, it has been demonstrated to be a very effective approximation of the low eigenmodes of an all-atom model [71, 37]. In this case, the total Hessian matrix is projected to a much smaller matrix [37],

$$H_{\text{proj}} = B^T H B,$$

where  $B \in \mathbb{R}^{N \times 6n} = [b_1, b_2, \dots, b_{6n}]$  is an orthogonal matrix (the number of atoms  $N \gg$  the number of blocks  $6n$ ), with each column representing a rotational or translational mode of a residue. The orthogonal matrix  $B$  is given by [71, 37]

$$B_{J,j\nu}^\mu = \begin{cases} \sqrt{\frac{m_j}{M_J}} \delta_{\mu\nu}, & \mu = 1, 2, 3; \\ \sum_{\alpha,\beta} I_{J\mu-3,\alpha}^{-1/2} \sqrt{m_j} (r_j - r_J^0)_\beta \epsilon_{\alpha\beta\nu}, & \mu = 4, 5, 6. \end{cases} \quad (7.5)$$

Here  $J$  and  $j$  subscript label blocks and atoms,  $\mu = 1, 2, 3$  and  $\mu = 4, 5, 6$  label translations and rotations,  $m_j$  and  $r_j$  label the mass and Cartesian coordinates of the atom  $j$ ,  $M_J$ ,  $I_J$ , and  $r_J^0$  label the total mass, moment of inertia, and center of mass of the block  $J$ ,  $\delta$  is the Kronecker delta, and  $\epsilon$  is the permutation over  $\alpha, \beta, \nu$  over  $\{1, 2, 3\}$ .

The low-eigen modes of  $H_{\text{proj}}$ , due to the much smaller dimension, can be computed with classical algorithms. For example, let  $\mathbf{w}$  be an eigenvector of  $H_{\text{proj}}$ . Then, we can choose,

$$|\psi_0\rangle = w_1 |b_1\rangle + w_2 |b_2\rangle + \dots + w_{6n} |b_{6n}\rangle.$$

The RTB approach has been demonstrated to be quite effective in approximating low eigenmodes [98, 71]. One way to quickly check whether the overlap between  $|\psi_0\rangle$  and  $|\psi\rangle$  is to compute the residual error. Consider  $E = \langle \psi_0 | H | \psi_0 \rangle$ , which is known as the Ritz value. Then

$$|\langle \psi_0 | \psi \rangle|^2 \geq 1 - \frac{\|H\psi_0 - E\psi_0\|^2}{\Delta^2}, \quad (7.6)$$

here  $\Delta$  refers to the spectral gap and the numerator is the residue error, which can be directly examined.

Overall, the RTB approach relies on a partition of the protein into more rigid structures to capture the low-lying eigenmodes. In addition to this natural choice of residues, one can also use other partition schemes, e.g, based on atomic density [37] or rigidity analysis [65].

Given an initial good guess  $|\psi_0\rangle$  as prepared above, we can filter out zero eigenstates by the projector  $P_{Y^\perp} = I - \sum_{v \in Y^\perp} \mathbf{v}\mathbf{v}^T$ , and then prepare the filtered initial state

$$|\psi'_0\rangle = \frac{P_{Y^\perp} |\psi_0\rangle}{\sqrt{\langle P_{Y^\perp} |\psi_0\rangle}}$$

The state  $|\psi'_0\rangle$  has zero overlap with the zero eigenspace  $Y$ , and has  $p_0$  overlap with the nonzero eigenstate  $|\psi\rangle = |\psi_6\rangle$ , where  $|\langle \psi_0 | \psi \rangle|^2 = p_0 \geq \gamma^2$ . We then use this state to prepare the first nonzero eigenvalue and eigenstate.

Lin and Tong developed LCU-based quantum eigenstate filtering method for the ground state preparation and energy estimation with near-optimal cost [76].

For the purpose of early fault-tolerant quantum algorithms, we can employ the QET-U approach, a modified QSP approach with a shorter quantum circuit.

**Theorem 7.3** (Theorem 11 of [43]). *Suppose we are given a Hamiltonian  $H$  on  $n$ -qubit whose spectrum is contained in  $[\eta, \pi - \eta]$ , for  $\eta > 0$ . Given the Hamiltonian evolution input  $U_H = e^{-iH}$ . Also suppose we have an initial state  $|\psi_0\rangle$  prepared by circuit  $U_I$ , with lower bound for the overlap:  $|\langle \psi_0 | \psi \rangle|^2 = p_0 \geq \gamma^2$ . Then the ground state energy can be prepared to precision  $\epsilon$  with probability  $1 - \delta$  with the following cost:*

- (i)  $\mathcal{O}\left(\frac{1}{\gamma\epsilon} \log(1/\delta)\right)$  queries to (controlled-)  $U_H$  and  $\mathcal{O}\left(\frac{1}{\gamma} \log(1/\delta)\right)$  queries to  $U_I$ ;
- (ii) three ancilla qubits;
- (iii)  $\mathcal{O}\left(\frac{1}{n\gamma} \log(1/(\delta\epsilon)) + \frac{1}{\gamma\epsilon} \log(1/\delta)\right)$  number of other one- or two-qubit gates;
- (iv)  $\mathcal{O}\left(\frac{1}{\gamma\epsilon} \log(1/\delta)\right)$  query depth of  $U_H$ .

For large overlap  $\gamma = \Omega(1)$ , we can employ a simple quantum circuit with classical post-processing procedure. The algorithm samples from Hadamard tests, and uses the samples to approximately reconstruct the cumulative distribution function (CDF) of the spectral measure associated with the Hamiltonian, and then estimate the ground state energy with high confidence.

Let the initial state be expanded as  $|\psi_0\rangle = \sum_k \alpha_k |\psi_k\rangle$  in the eigenbasis of  $H$ , and let  $p_k = |\alpha_k|^2$  be the overlap with the  $k$ -th eigenstate. They considered the spectral density function  $p(x) = \sum_k p_k \delta(x - \lambda_k)$  and its cumulative distribution function (CDF)  $C(x) = \int_x p(x) dx$ . The algorithm in [78] aims to estimate  $\lambda_0$  by locating the first nonzero point of  $C(x)$ . In our case, when we choose  $|\phi'_0\rangle = \frac{P_{Y^\perp} |\psi_0\rangle}{\sqrt{\langle P_{Y^\perp} |\psi_0\rangle}}$ , we observe that  $p_0 = p_1 = \dots = p_5 = 0$ . So we can straightforwardly perform the quantum eigenvalue estimation algorithm in [78] to estimate  $\lambda_6$ .

**Theorem 7.4** (Corollary 3 of [78]). *Suppose we have an initial state  $|\psi_0\rangle$  prepared by circuit  $U_I$ , with lower bound for the overlap:  $|\langle \psi_0 | \psi \rangle|^2 = p_0 \geq \gamma^2$ . There is a quantum algorithm that estimates*

the ground state energy and prepares the ground state to precision  $\epsilon$  with probability  $1 - \delta$  with the following cost

- (i)  $\mathcal{O}\left(\frac{1}{\gamma^4 \epsilon} \log(1/\delta)\right)$  queries to (controlled-) $U_H$  and  $\mathcal{O}\left(\frac{1}{\gamma^4} \log(1/\delta)\right)$  queries to  $U_I$ ;
- (ii)  $\mathcal{O}(1)$  ancilla qubits;
- (iii)  $\mathcal{O}\left(\frac{1}{\gamma^4 \epsilon} \log(1/\delta)\right)$  number of other one- or two-qubit gates;
- (iv)  $\mathcal{O}\left(\frac{1}{\epsilon} \log\left(\frac{1}{\gamma \nu}\right)\right)$  query depth of  $U_H$ ;

and classical post-processing cost  $\mathcal{O}\left(\frac{1}{p_0^2} \text{polylog}\left(\frac{1}{p_0 \epsilon}\right)\right)$ .

For example, the approaches in [46, 75] usually extract multiple normal modes as a starting point to study the actual dynamics of proteins.

We may investigate other early fault-tolerant quantum algorithms, such as QET-U [43], QCELS [39, 40], and RPE [88, 72]. But if we aim to estimate multiple eigenstates and eigenvalues, we intend to employ MM-QCELS [40] and RMPE [72].

### 7.3 Density of States and Chebyshev moments

Here we discuss the estimation of the density of states (DoS), given by,

$$\varrho(\lambda) = \frac{1}{N} \sum_{j=0}^{N-1} \delta(\lambda - \lambda_j), \quad (7.7)$$

for the eigenvalue distribution of the adjacency matrix of the protein network [64]. Specifically,  $\{\lambda_j\}$  are eigenvalues of the Hamiltonian  $H$ , associated with eigenvectors  $\{|\psi_j\rangle\}$ . We are given an  $\alpha$ -block-encoding of  $H$ . More generally, we can estimate the local density of the state

$$\varrho_{\vec{r}}(\lambda) = \frac{1}{N} \sum_{j=0}^{N-1} \delta(\lambda - \lambda_j) |\langle \psi_j | \vec{r} \rangle|^2. \quad (7.8)$$

Notice that the density of states (7.7) can be obtained from the local density of states by integration over  $\vec{r}$ .

In general, we can consider a function  $f(\lambda)$  defined via an observable  $A$

$$f(\lambda) = \sum_{j=0}^{N-1} \delta(\lambda - \lambda_j) \langle \psi_j | A | \psi_j \rangle. \quad (7.9)$$

We approach this problem by computing the integral of  $f$  over an interval  $[a, b]$ , specifically, the moments of a Chebyshev expansion of  $f(\lambda)$ , as we show below. Following [92], there exists a

polynomial  $w(x)$  that has degree  $d = \mathcal{O}(\frac{f_{\max}}{\epsilon} \log \frac{f_{\max}}{\epsilon})$  and satisfies  $|w(x)| \leq 1$ , such that

$$\begin{aligned} \int_a^b f(\lambda) d\lambda &\approx \alpha \int_{-1}^1 f(\alpha x) w(x) dx = \int_{-1}^1 \sum_{j=0}^{N-1} \delta(\alpha x - \lambda_j) \langle \psi_j | A | \psi_j \rangle w(x) dx \\ &= \text{Tr} \left( A \sum_{j=0}^{N-1} \int_{-1}^1 \delta(x - \lambda_j / \alpha) w(x) | \psi_j \rangle \langle \psi_j | \right) \\ &= \text{Tr} \left( A \sum_{j=0}^{N-1} w(\lambda_j / \alpha) | \psi_j \rangle \langle \psi_j | \right) = \text{Tr} \left( A w(H / \alpha) \right). \end{aligned} \quad (7.10)$$

We then calculate the moments of  $f(\lambda)$  based on Chebyshev polynomial of the first kind  $T_k(x)$

$$\mu_k^f = \int_a^b T_k(x) f(\alpha x) dx, \quad (7.11)$$

and from the calculations above, we find,

$$\mu_k^f \approx \text{Tr} \left( A T_k(H / \alpha) \right). \quad (7.12)$$

To compute the density of state  $\rho(\lambda)$  (7.7), we choose  $A = I/N$  in  $f(\lambda)$ , such that

$$\int_a^b \rho(\lambda) d\lambda \approx \text{Tr} \left( \frac{I}{N} w(H / \alpha) \right), \quad (7.13)$$

$$\mu_k^\rho \approx \text{Tr} \left( \frac{I}{N} T_k(H / \alpha) \right). \quad (7.14)$$

The observable estimation lemma [92] is stated as below.

**Lemma 7.5** (Lemma 5 of [92]). *Let  $U_A$  be an  $\alpha$ -block-encoding of the Hermitian matrix  $A$  and  $U_A$  can be implemented with  $Q$  elementary gates. Let  $U_I$  prepare  $\rho$  with  $R$  elementary gates. For  $\epsilon > 0$ , there is a quantum algorithm that estimates  $\text{Tr}(A\rho)$  within  $\epsilon$  with probability  $\Omega(1)$  with gate complexity  $\mathcal{O}((R + Q)\frac{\alpha}{\epsilon})$ .*

Given a  $\alpha$ -block-encoding of the Hermitian  $A$ , there is a  $(\alpha d)$ -block-encoding of  $f(A)$ , where  $f$  is a  $d$ -degree polynomial. We use the lemma below to present the complexity results.

**Theorem 7.6** (Theorem 11 of [92]). *Let  $U_H$  be an  $\alpha$ -block-encoding of the Hermitian  $H$ . For any  $\epsilon, \delta > 0$ :*

1. *There exists a quantum algorithm that estimates  $\int_a^b \rho(\lambda) d\lambda$  with  $\mathcal{O}(\frac{\alpha \varrho_{\max}}{\epsilon^2})$  queries to  $U_H$  and overall quantum gate complexity  $\mathcal{O}\left(\left(\frac{\alpha \varrho_{\max}}{\epsilon} + \log N\right) \cdot \frac{\log(1/\delta)}{\epsilon}\right)$  and classical pre-processing  $\mathcal{O}(\text{poly}(\frac{\varrho_{\max}}{\epsilon}))$ , where  $\varrho_{\max}$  is an upper bound of the dimension of the largest eigenspace of  $H$ .*
2. *There exists a quantum algorithm that estimates  $\mu_k^\rho$  with  $\mathcal{O}(\frac{\alpha n}{\epsilon})$  queries to  $U_H$  and overall quantum gate complexity  $\mathcal{O}\left((\alpha k + \log N) \cdot \frac{\log(1/\delta)}{\epsilon}\right)$ , where  $k$  is the degree of Chebyshev polynomial.*

The above algorithm can be extended to the local density of states in Eq. (7.8). This can come up when we are working with a Hamiltonian describing a single particle in real space or some space with a notion of locality. For every position  $\vec{r}$ , there is a state  $|\psi(\vec{r})\rangle$  denoting the state with the particle at  $\vec{r}$ . The algorithms for estimating the LDOS are a simple modification of the algorithms for DOS: instead of preparing a maximally mixed state we simply prepare  $|\psi(\vec{r})\rangle$ . If  $|\psi(\vec{r})\rangle$  has a  $O(R)$  preparation unitary, the new circuit complexities are the same as those in [Theorem 7.6](#) but with  $\log D$  replaced with  $R$ .

An alternative definition of the local density of the state is given by

$$\varrho_{\vec{r}}(\lambda) = \frac{1}{N} \sum_{j=0}^{N-1} \delta(\lambda - \lambda_j) |\langle \psi_j(\vec{r}) | \psi(\vec{r}) \rangle|^2. \quad (7.15)$$

The contribution of each state is weighted by the density of its wave function at the point  $\vec{r}$ . We can further generalize the local density of states further to

$$\varrho_{\vec{r}, \vec{r}'}(\lambda) = \frac{1}{N} \sum_{j=0}^{N-1} \delta(\lambda - \lambda_j) |\langle \psi_j(\vec{r}) | \psi_j(\vec{r}') \rangle|^2. \quad (7.16)$$

This is called the spectral function and it is a function with each wave function evaluated as a different position. It can be interpreted as a Green's function. This type of function can also be treated using a similar quantum algorithm.

## 7.4 Correlation and root mean square of displacement

In this section, we develop quantum algorithms for estimating the cross-correlation and root mean square of the atomic displacement based on the block-encoding of the pseudo-inverse of the Hamiltonian.

Let  $\omega_k^2$  be the  $k$ th eigenvalue of  $H$  with eigenvector  $\mathbf{v}_k$ . Then  $H$  admits the following spectral decomposition,

$$H = \sum_{k=7}^{3N} \omega_k^2 \mathbf{v}_k \mathbf{v}_k^T. \quad (7.17)$$

Recall that the first six eigenvalues of  $H$  are zero. Therefore, the pseudo-inverse is given by,

$$H^- = \sum_{k=7}^{3N} \frac{1}{\omega_k^2} \mathbf{v}_k \mathbf{v}_k^T. \quad (7.18)$$

We can efficiently block encode the (pseudo) inverse of Hamiltonian  $H$ . According to [\[96, 50, 97\]](#), we have the following result.

**Lemma 7.7** (Proposition 9 of [\[97\]](#)). *Let  $H$  be a Hermitian matrix that its eigenvalues is on  $[-\alpha, -1/\beta] \cup [1/\beta, \alpha]$ , with condition number  $\kappa = \alpha\beta$ . Given  $U_H$  that is a  $(\alpha, a, \epsilon)$ -block-encoding of  $H$ , we can implement  $U^-$  that is a  $(\beta', a + 2, \epsilon')$ -block-encoding of  $H^-$  with  $\beta' = \frac{16}{3}\beta$ ,  $\epsilon' = 4d(\sqrt{\frac{\epsilon}{\alpha} + \delta})\beta'$ , which consists of  $\mathcal{O}(d)$  uses of  $U_H$  and  $\mathcal{O}((a + 1)d)$  uses of additional one- or two-qubit gates, where  $d = \mathcal{O}(\kappa \log(1/\delta))$ .*

Given the block-encoded (inverse) Hamiltonian, we can use amplitude estimation to estimate the expectation of block-encoded observables.

Based on the observable estimation lemma as in [Lemma 7.5](#), we have  $\alpha = 1/\beta$ , and  $Q = \mathcal{O}(d) = \mathcal{O}(\kappa \log(1/\delta))$ . Therefore, we can estimate  $\text{Tr}(H^- \rho)$  for certain observable  $\rho$  with gate complexity  $\mathcal{O}((R + d) \frac{1}{\beta \epsilon}) = \mathcal{O}(\frac{R}{\beta \epsilon} + \frac{\alpha}{\epsilon} \log(1/\delta))$ .

Meanwhile, often of interest is the cross-correlation of the atomic displacement, i.e.,

$$\mathbb{E}[\mathbf{u}_i \mathbf{u}_j]. \quad (7.19)$$

One can show that the cross-correlation can be expressed in terms of the matrix inverse,

$$\mathbb{E}[\mathbf{u}_i \mathbf{u}_j] = H_{ij}^- = \text{Tr}(H^- |j\rangle \langle i|). \quad (7.20)$$

Therefore, we can perform the observable estimation with  $\rho = |j\rangle \langle i|$ . Although the probability of measuring a single index  $|j\rangle \langle i|$  is small (i.e. it is highly likely to return the zero result), we can estimate a collection of indices  $\rho = \sum_{(i,j) \in \mathcal{I}} |j\rangle \langle i|$ .

Another important statistical quantity is the root mean square displacement [\[41\]](#). which is related to the eigenvalues as follows,

$$\text{RMSE} = \sqrt{\frac{1}{N} \sum_j \mathbb{E}[\mathbf{u}_j^2]} = \sqrt{\frac{1}{N} \sum_k \frac{1}{\omega_k^2}}. \quad (7.21)$$

We can perform amplitude estimation to produce  $\text{Tr}(H^- \rho)$  with  $\rho = I$ .

We summarize the results as follows.

**Theorem 7.8.** *Let  $U_H$  be an  $\alpha$ -block-encoding of the Hermitian  $H$  and  $U_H$  can be implemented with  $R$  elementary gates. Let  $U_I$  prepare  $\rho = \sum_{(i,j) \in \mathcal{I}} |j\rangle \langle i|$  with  $R$  elementary gates. For any  $\epsilon > 0$ :*

1. *There exists a quantum algorithm that estimates the cross-correlation of displacement  $\sum_{(i,j) \in \mathcal{I}} \mathbb{E}[\Delta R_i \Delta R_j]$  within  $\epsilon$ , with gate complexity  $\mathcal{O}\left(\frac{R}{\beta \epsilon} + \frac{\alpha}{\epsilon}\right)$ .*
2. *There exists a quantum algorithm that estimates the root mean square of displacement  $\sqrt{\frac{1}{N} \sum_j \mathbb{E}[\Delta R_j^2]}$  within  $\epsilon$  with gate complexity  $\mathcal{O}\left(\frac{R}{\beta \epsilon} + \frac{\alpha}{\epsilon}\right)$ .*

## 7.5 Molecular dynamic control

We combine the optimal control theory and molecular dynamics for protein folding problems [\[7\]](#).

The general Linear-Quadratic-Regulator (LQR) problems can be formulated based on a driven ODE,

$$\frac{d}{dt} \mathbf{x}(t) = A \mathbf{x}(t) + B \mathbf{u}(t). \quad (7.22)$$

For the molecular dynamical control, the course-grained folding dynamics is governed by the equation of motion

$$M \frac{d^2 \mathbf{u}(t)}{dt^2} + \gamma \frac{d \mathbf{u}(t)}{dt} + K \mathbf{u}(t) = \mathbf{f}(t). \quad (7.23)$$

Here  $M$  is the mass,  $\gamma$  is the friction,  $K$  is the connectivity matrix, and  $F$  is the  $n$ -dimensional force field. For instance, we have access to control  $F$  with a low dimensional input  $u = [u_1, \dots, u_m]^T$  ( $m \ll n$ ), such that  $u(t) = \sum_{j=1}^m u_j(t)e_j$ , where  $e_j$  is a fixed vector. Here we can reformulate the equation of motion as the ODE with new variable  $\mathbf{x}(t) = [R(t), \dot{R}(t)]$ .

In addition, the cost function can be defined either over an infinite horizon ( $T = +\infty$ ) or a finite horizon. In the latter case, the cost function is defined as,

$$J[\mathbf{f}] = \frac{1}{2}\mathbf{u}(T)^T S\mathbf{u}(T) + \int_0^T \mathbf{u}(t)^T Q\mathbf{u}(t) + \mathbf{f}(t)^T R\mathbf{f}(t)dt. \quad (7.24)$$

A convenient framework for computing the gradient of  $J$  with respect to the control variable is the Lagrange multiplier approach [67, Part IV], which expresses the gradient through an adjoint equation,

$$\frac{d}{dt}\mathbf{y}(t) = A\mathbf{y}(t) - Q\mathbf{x}(t), \quad \mathbf{y}(T) = S\mathbf{x}(T). \quad (7.25)$$

Notice that this equation has to be solved backward in time using a terminal condition at time  $T$ . With the Lagrange multiplier,  $\mathbf{y}(t)$ , the gradient is given by,

$$\frac{\delta J}{\delta \mathbf{u}(t)} = R\mathbf{u}(t) + B^T \mathbf{y}(t), \quad (7.26)$$

which can be incorporated into a gradient-based optimization algorithm, e.g., gradient descent or quasi-Newton's method [73].

**Theorem 7.9.** *For the protein dynamics (7.23) with cost function (7.24), let  $V$  be an  $\beta$ -block-encoding of the observable  $O$ . There exists a quantum algorithm that estimates the output  $J$  within  $\epsilon$ , with  $\mathcal{O}(\frac{\beta \log(1/\delta)}{\epsilon})$  uses of  $V$  and the quantum algorithm  $U(t)$  that prepares  $|\psi(t)\rangle$  in Theorem 6.1.*

## 8 Numerical experiments

We have designed several numerical experiments to test some of our algorithms. As examples, we estimate the density of states using the Chebyshev moments (Theorem 7.6) approach and find the optimal control in the (Theorem 7.9) problem. These tests are conducted on classical devices to demonstrate the feasibility of the algorithms.

### 8.1 Estimating the density of states

To demonstrate the DoS calculation, we consider a Crambin protein, consisting of 1360 atoms with the molecular structure shown in Fig. 1. For this molecule, we used the Tinker package [91], and estimated the Hessian matrix  $K$  and the mass matrix  $M$  as input to estimate protein properties. To verify the potential efficiency in uploading the  $K$ , we show the sparsity pattern of the matrix in Fig. 2 using a cut-off distance of Å. As highlighted in (Theorem 7.6), the DoS can be estimated through the generalized moments in Eq. (7.14). To mimic the estimation of the corresponding observables, we use a stochastic estimation as follows,

$$\mu_k = \mathbb{E}[\langle \phi | T_k(H) | \phi \rangle], \quad (8.1)$$



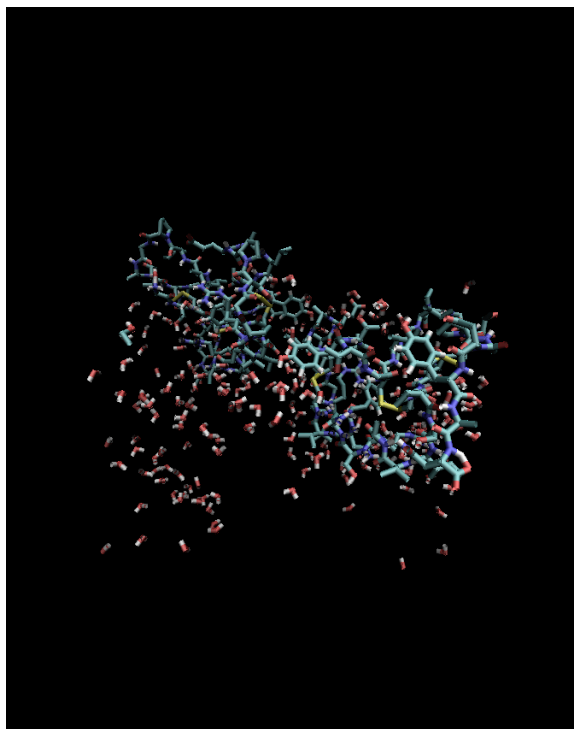


Figure 1: The molecular configuration of Crambin.

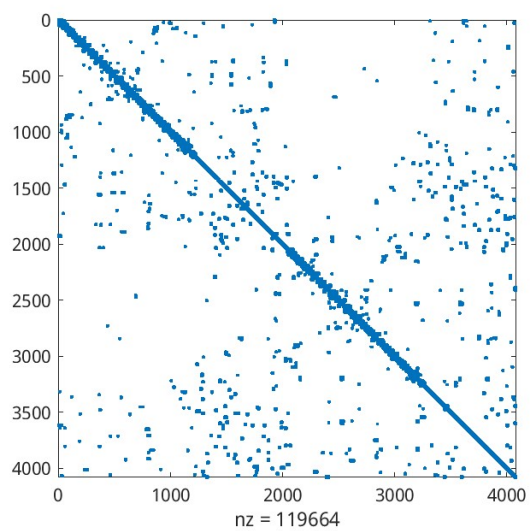


Figure 2: The sparse pattern of the connectivity matrix by using a cut-off distance of  $\text{\AA}$ .

where the entries of  $|\phi\rangle$  are sampled from Gaussian random variables, so that Eq. (8.1) is a consistent estimator of Eq. (7.14). In Figure 3, we show the moments computed from (8.1) and compare them with the exact values obtained from brute force matrix multiplications. Surprisingly, estimating these moments only requires a small number of samples.

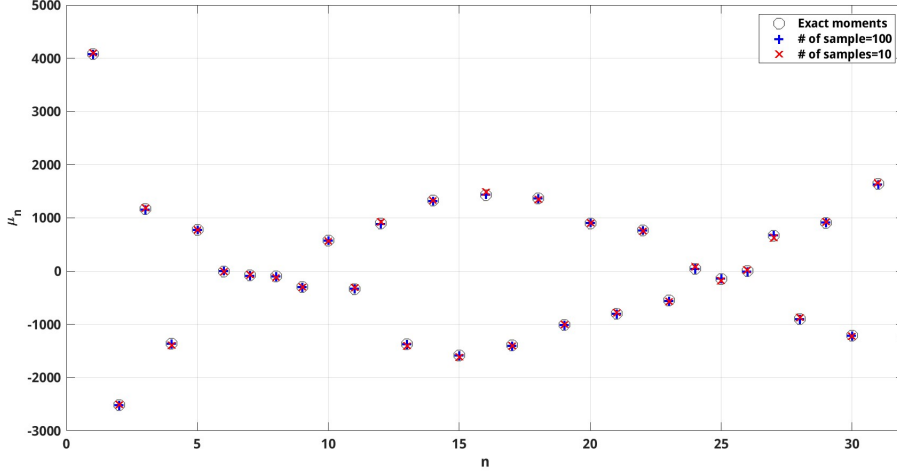


Figure 3: Comparison of the exact moments and the approximate moments computed from random samples in (8.1).

Using the moments, we have estimated the density of states, shown in Fig. 4. For the moments in (7.12), we have used 1024 moments each computed with 100 samples. We observe a good agreement with the histogram of the eigenvalues (computed with direct diagonalization).

## 8.2 Protein folding using LQR control

In our next numerical experiment, we follow the approach in [7] and study the folding mechanism via an LQR control. In general, LQR involves the following feedback control of a linear ODE system,

$$E\mathbf{y}' = A\mathbf{y} + B\mathbf{u}(t). \quad (8.2)$$

The goal is to determine the control signals  $\mathbf{u}(t)$  to minimize the cost function,

$$J[\mathbf{u}] = \int_0^T \mathbf{y}(t)^T Q \mathbf{y}(t) + \mathbf{u}(t)^T R \mathbf{u}(t) dt. \quad (8.3)$$

Furthermore, to cast the dynamics (7.23) into the form (8.2), we define a combined variable  $\mathbf{y} = [R \quad \dot{R}]^T$  and choose,

$$A = \begin{bmatrix} \mathbf{0} & I \\ -K & -\gamma I \end{bmatrix}, \quad E = \begin{bmatrix} I & \mathbf{0} \\ \mathbf{0} & M \end{bmatrix},$$

where we have defined the matrix  $B$  so that  $\mathbf{u}(t)$  only acts on the  $C - \alpha$  atoms. They are regarded

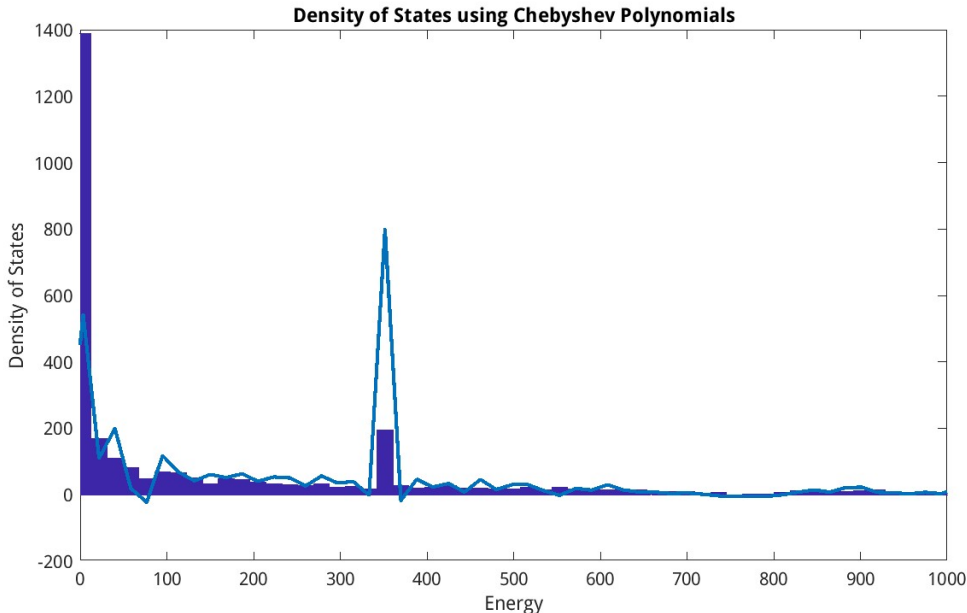


Figure 4: Comparison of the density of states estimated from the Chebyshev moments with the histogram of the eigenvalues.

as forces that steer the system toward its native state. Namely,

$$B = \begin{bmatrix} \mathbf{0} \\ \tilde{B} \end{bmatrix},$$

where  $\tilde{B}_{i,j} = 1$ , if  $i$ th atom is the  $j$ th  $C_\alpha$  atom, and zero otherwise. For the cost function, we choose a block diagonal matrix for  $Q$  so that,  $\mathbf{y}(t)^T Q \mathbf{y}(t)$  corresponds to the total energy: Minimizing the energy will steer the system toward an equilibrium state. We choose  $R = I$ . As a specific example, we perform the simulations on a Chignolin protein.

We performed an LQR control with a finite horizon. We start with an initial state away from the equilibrium. To determine the control  $u(t)$ , we solve the forward and the adjoint equations to estimate the gradient. For the iterations of  $u(t)$ , we use the BFGS algorithms. As a specific example, we consider a Chignolin protein and starting configuration away from equilibrium, followed by a control algorithm that minimizes the energy [7]. Figure 5 shows the resulting potential energy in time, which shows that the molecule has been guided back to equilibrium. In the upper panel, we also show the snapshots of the molecular structure following the time-dependent control.

## 9 Discussion and outlook

In this work, motivated by the critical role of protein dynamics in biology, we conducted a systematic study of quantum computing algorithms for simulating protein dynamics and the resulting properties. Our focus is on end-to-end quantum algorithms for simulating various protein dynam-

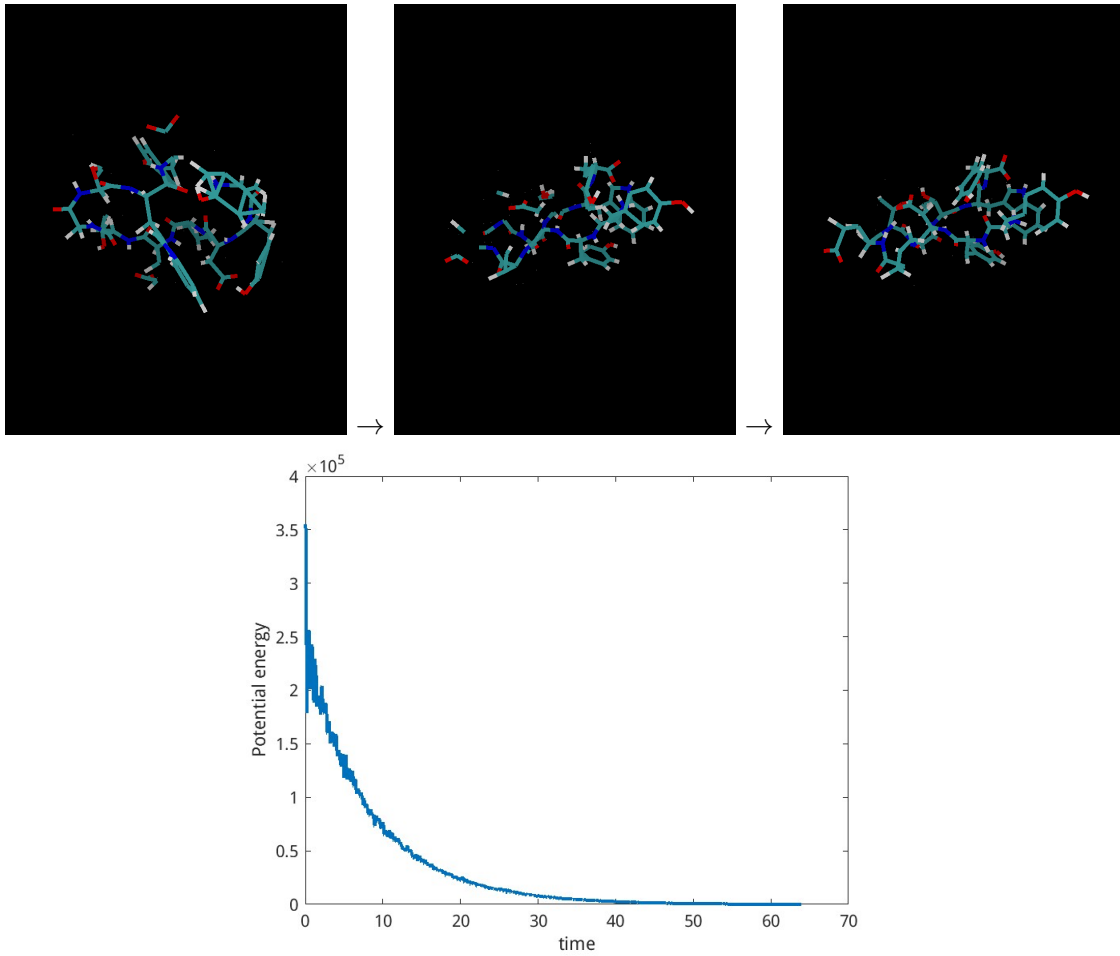


Figure 5: Top: the structural changes under the control; Bottom: The total energy  $\mathbf{y}(t)^T Q \mathbf{y}(t)$  following the optimal control  $\mathbf{u}(t)$ .

ical models. We present a detailed analysis of the computational complexity of these quantum simulation algorithms, as well as the quantum protocols for data input (read-in) and output (read-out). Additionally, we discuss several concrete applications and illustrate the potential efficiency of these algorithms through classical numerical experiments.

Our work also indicates natural open questions for future investigation.

- Can we develop even faster quantum algorithms for certain protein problems, by employing fast-forwarded Hamiltonian simulations or quantum linear ODE solvers?
- How to prove quantum lower bounds of the quantum simulation for protein dynamics, in the sense of parameters such as the evolution time, error tolerance, and number of particles? Moreover, can we establish a solid classical lower bound for an end-to-end problem, such that there is a rigorous end-to-end exponential quantum speedup over classical algorithms?
- The current algorithms are designed to capture dynamics due to vibration modes. How to generalize the quantum algorithms for more practical molecular dynamics, e.g., ab initio molecular dynamics? In particular, can nonlinear dynamics be simulated using appropriate embedding techniques, such as Carleman or Koopman embedding [82]?
- Can we offer more practical matrix connectivity loading protocols for uploading the protein information, without utilizing circuit-based QROM?
- Can we use the initial state preparation algorithm based on rejection sampling to produce other useful quantum states with pseudo-random amplitudes?

## References

- [1] J. Allcock, J. Bao, J. F. Doriguello, A. Luongo, and M. Santha. Constant-depth circuits for uniformly controlled gates and Boolean functions with application to quantum memory circuits, 2023. [arXiv:2308.08539](#).
- [2] A. Ambainis. Variable time amplitude amplification and quantum algorithms for linear algebra problems. In *29th Symposium on Theoretical Aspects of Computer Science*, volume 14, pages 636–647. LIPIcs, 2012. [arXiv:1010.4458](#).
- [3] D. An, A. M. Childs, and L. Lin. Quantum algorithm for linear non-unitary dynamics with near-optimal dependence on all parameters, 2023. [arXiv:2312.03916](#).
- [4] D. An and L. Lin. Quantum linear system solver based on time-optimal adiabatic quantum computing and quantum approximate optimization algorithm. *ACM Transactions on Quantum Computing*, 3(2):1–28, Jun 2022. [arXiv:1909.05500](#).
- [5] D. An, J.-P. Liu, and L. Lin. Linear combination of Hamiltonian simulation for nonunitary dynamics with optimal state preparation cost. *Physical Review Letters*, 131(15):150603, 2023. [arXiv:2303.01029](#).

- [6] D. An, J.-P. Liu, D. Wang, and Q. Zhao. A theory of quantum differential equation solvers: limitations and fast-forwarding, 2022. [arXiv:2211.05246](#).
- [7] Y. Arkun and M. Gur. Combining optimal control theory and molecular dynamics for protein folding. *PLoS One*, 7(1):e29628, 2012.
- [8] S. Arunachalam, V. Gheorghiu, T. Jochym-O’Connor, M. Mosca, and P. V. Srinivasan. On the robustness of bucket brigade quantum RAM. *New Journal of Physics*, 17(12):123010, 2015. [arXiv:1502.03450](#).
- [9] N. W. Ashcroft and N. D. Mermin. *Solid state physics*. Cengage Learning, 2022.
- [10] A. R. Atilgan, S. Durell, R. L. Jernigan, M. C. Demirel, O. Keskin, and I. Bahar. Anisotropy of fluctuation dynamics of proteins with an elastic network model. *Biophysical journal*, 80(1):505–515, 2001.
- [11] R. Babbush, D. W. Berry, R. Kothari, R. D. Somma, and N. Wiebe. Exponential quantum speedup in simulating coupled classical oscillators. *Physical Review X*, 13(4):041041, 2023. [arXiv:2303.13012](#).
- [12] R. Babbush, C. Gidney, D. W. Berry, N. Wiebe, J. McClean, A. Paler, A. Fowler, and H. Neven. Encoding electronic spectra in quantum circuits with linear t complexity. *Physical Review X*, 8(4):041015, 2018. [arXiv:1805.03662](#).
- [13] R. Babbush, A. Perdomo-Ortiz, B. O’Gorman, W. Macready, and A. Aspuru-Guzik. Construction of energy functions for lattice heteropolymer models: Efficient encodings for constraint satisfaction programming and quantum annealing. *Advances in Chemical Physics: Volume 155*, pages 201–244, 2014. [arXiv:1211.3422](#).
- [14] I. Bahar, A. R. Atilgan, and B. Erman. Direct evaluation of thermal fluctuations in proteins using a single-parameter harmonic potential. *Folding and Design*, 2(3):173–181, 1997.
- [15] D. Ben-Avraham. Vibrational normal-mode spectrum of globular proteins. *Physical Review B*, 47(21):14559, 1993.
- [16] D. W. Berry. High-order quantum algorithm for solving linear differential equations. *Journal of Physics A: Mathematical and Theoretical*, 47(10):105301, 2014. [arXiv:1010.2745](#).
- [17] D. W. Berry, G. Ahokas, R. Cleve, and B. C. Sanders. Efficient quantum algorithms for simulating sparse Hamiltonians. *Communications in Mathematical Physics*, 270:359–371, 2007. [arXiv:quant-ph/0508139](#).
- [18] D. W. Berry, A. M. Childs, R. Cleve, R. Kothari, and R. D. Somma. Simulating Hamiltonian dynamics with a truncated Taylor series. *Physical Review Letters*, 114(9):090502, 2015. [arXiv:1412.4687](#).

- [19] D. W. Berry, A. M. Childs, R. Cleve, R. Kothari, and R. D. Somma. Exponential improvement in precision for simulating sparse Hamiltonians. In *Forum of Mathematics, Sigma*, volume 5. Cambridge University Press, 2017. [arXiv:1312.1414](#).
- [20] D. W. Berry, A. M. Childs, A. Ostrander, and G. Wang. Quantum algorithm for linear differential equations with exponentially improved dependence on precision. *Communications in Mathematical Physics*, 356(3):1057–1081, 2017. [arXiv:1701.03684](#).
- [21] D. W. Berry and P. C. Costa. Quantum algorithm for time-dependent differential equations using Dyson series. *Quantum*, 8:1369, 2024. [arXiv:2212.03544](#).
- [22] D. Bluvstein, S. J. Evered, A. A. Geim, S. H. Li, H. Zhou, T. Manovitz, S. Ebadi, M. Cain, M. Kalinowski, D. Hangleiter, et al. Logical quantum processor based on reconfigurable atom arrays. *Nature*, pages 1–3, 2023. [arXiv:2312.03982](#).
- [23] S. Bopardikar, K. Dasgupta, S. Senapati, et al. An approach to solve the coarse-grained protein folding problem in a quantum computer, 2023. [arXiv:2311.14141](#).
- [24] A. Bouland, A. Dandapani, and A. Prakash. A quantum spectral method for simulating stochastic processes, with applications to Monte Carlo, 2023. [arXiv:2303.06719](#).
- [25] G. Brassard, P. Hoyer, M. Mosca, and A. Tapp. Quantum amplitude amplification and estimation. *Contemporary Mathematics*, 305:53–74, 2002. [arXiv:quant-ph/0005055](#).
- [26] H.-P. Breuer and F. Petruccione. *The theory of open quantum systems*. Oxford University Press, USA, 2002.
- [27] C.-F. Chen, M. J. Kastoryano, F. G. Brandão, and A. Gilyén. Quantum thermal state preparation. 2023. [arXiv:2303.18224](#).
- [28] C. Chennubhotla and I. Bahar. Markov propagation of allosteric effects in biomolecular systems: application to groel-groes. *Molecular systems biology*, 2(1):36, 2006.
- [29] C. Chennubhotla and I. Bahar. Markov methods for hierarchical coarse-graining of large protein dynamics. *Journal of computational biology*, 14(6):765–776, 2007.
- [30] A. M. Childs, R. Kothari, and R. D. Somma. Quantum algorithm for systems of linear equations with exponentially improved dependence on precision. *SIAM Journal on Computing*, 46(6):1920–1950, 2017. [arXiv:1511.02306](#).
- [31] A. M. Childs and T. Li. Efficient simulation of sparse Markovian quantum dynamics. *Quantum Information & Computation*, 17(11&12):0901–0947, 2017. [arXiv:1611.05543](#).
- [32] A. M. Childs and J.-P. Liu. Quantum spectral methods for differential equations. *Communications in Mathematical Physics*, 375:1427–1457, 2020. [arXiv:1901.00961](#).

- [33] A. M. Childs, J.-P. Liu, and A. Ostrander. High-precision quantum algorithms for partial differential equations. *Quantum*, 5:574, 2021. [arXiv:2002.07868](#).
- [34] R. Cleve and C. Wang. Efficient quantum algorithms for simulating Lindblad evolution. In *Proceedings of the 44th International Colloquium on Automata, Languages, and Programming (ICALP 2017)*, pages 17:1–17:14, 2017. [arXiv:1612.09512](#).
- [35] A. Cornelissen, Y. Hamoudi, and S. Jerbi. Near-optimal quantum algorithms for multivariate mean estimation. In *Proceedings of the 54th Annual ACM SIGACT Symposium on Theory of Computing*, pages 33–43, 2022. [arXiv:2111.09787](#).
- [36] P. C. S. Costa, S. Jordan, and A. Ostrander. Quantum algorithm for simulating the wave equation. *Physical Review A*, 99(1):012323, 2019. [arXiv:1711.05394](#).
- [37] O. N. A. Demerdash and J. C. Mitchell. Density-cluster NMA: A new protein decomposition technique for coarse-grained normal mode analysis. *Proteins: Structure, Function, and Bioinformatics*, 80(7):1766–1779, 2012.
- [38] Z. Ding, X. Li, and L. Lin. Simulating open quantum systems using Hamiltonian simulations. *PRX Quantum*, 5(2):020332, 2024. [arXiv:2311.15533](#).
- [39] Z. Ding and L. Lin. Even shorter quantum circuit for phase estimation on early fault-tolerant quantum computers with applications to ground-state energy estimation. *PRX Quantum*, 4(2):020331, 2023. [arXiv:2211.11973](#).
- [40] Z. Ding and L. Lin. Simultaneous estimation of multiple eigenvalues with short-depth quantum circuit on early fault-tolerant quantum computers. *Quantum*, 7:1136, 2023. [arXiv:2303.05714](#).
- [41] S. E. Dobbins, V. I. Lesk, and M. J. Sternberg. Insights into protein flexibility: the relationship between normal modes and conformational change upon protein–protein docking. *Proceedings of the National Academy of Sciences*, 105(30):10390–10395, 2008.
- [42] H. Doga, B. Raubenolt, F. Cumbo, J. Joshi, F. P. DiFilippo, J. Qin, D. Blankenberg, and O. Shehab. A perspective on protein structure prediction using quantum computers, 2023. [arXiv:2312.00875](#).
- [43] Y. Dong, L. Lin, and Y. Tong. Ground-state preparation and energy estimation on early fault-tolerant quantum computers via quantum eigenvalue transformation of unitary matrices. *PRX Quantum*, 3(4):040305, 2022. [arXiv:2204.05955](#).
- [44] P. Doruker, R. L. Jernigan, and I. Bahar. Dynamics of large proteins through hierarchical levels of coarse-grained structures. *Journal of computational chemistry*, 23(1):119–127, 2002.



- [45] P. Durand, G. Trinquier, and Y.-H. Sanejouand. A new approach for determining low-frequency normal modes in macromolecules. *Biopolymers: Original Research on Biomolecules*, 34(6):759–771, 1994.
- [46] J. Elezgaray and Y.-H. Sanejouand. Modal dynamics of proteins in water. *Journal of Computational Chemistry*, 21(14):1274–1282, 2000.
- [47] M. Fingerhuth, T. Babej, et al. A quantum alternating operator ansatz with hard and soft constraints for lattice protein folding, 2018. [arXiv:1810.13411](#).
- [48] D. Frenkel and B. Smit. *Understanding molecular simulation: from algorithms to applications*. Elsevier, 2023.
- [49] E. Fuglebakk, N. Reuter, and K. Hinsen. Evaluation of protein elastic network models based on an analysis of collective motions. *Journal of chemical theory and computation*, 9(12):5618–5628, 2013.
- [50] A. Gilyén, Y. Su, G. H. Low, and N. Wiebe. Quantum singular value transformation and beyond: exponential improvements for quantum matrix arithmetics. In *Proceedings of the 51st Annual ACM SIGACT Symposium on Theory of Computing*, pages 193–204, 2019. [arXiv:1806.01838](#).
- [51] V. Giovannetti, S. Lloyd, and L. Maccone. Quantum random access memory. *Physical review letters*, 100(16):160501, 2008. [arXiv:0708.1879](#).
- [52] F. Golse, S. Jin, and N. Liu. Quantum algorithms for uncertainty quantification: application to partial differential equations, 2022. [arXiv:2209.11220](#).
- [53] L. Grover and T. Rudolph. Creating superpositions that correspond to efficiently integrable probability distributions, 2002. [arXiv:quant-ph/0208112](#).
- [54] T. Haliloglu, I. Bahar, and B. Erman. Gaussian dynamics of folded proteins. *Physical review letters*, 79(16):3090, 1997.
- [55] Y. Hamoudi. Quantum sub-Gaussian mean estimator. In *29th Annual European Symposium on Algorithms (ESA 2021)*. Schloss Dagstuhl-Leibniz-Zentrum für Informatik, 2021. [arXiv:2108.12172](#).
- [56] A. W. Harrow, A. Hassidim, and S. Lloyd. Quantum algorithm for linear systems of equations. *Physical Review Letters*, 103(15):150502, 2009. [arXiv:0811.3171](#).
- [57] M. Hu, S. Raj, B. Kim, W. K. Liu, S. Baik, T. Kim, B.-S. Lim, and M. K. Kim. Precise spring constant assignment in elastic network model for identification of vibration frequency and modeshape. *Journal of mechanical science and technology*, 24:1771–1780, 2010.

- [58] M.-W. Hu, B. O’Riordan, B. Kim, and M. K. Kim. Comparison of all-atom and coarse-grained normal mode analysis in the elastic network model. *Journal of Mechanical Science and Technology*, 27:3267–3275, 2013.
- [59] A. Irbäck, L. Knuthson, S. Mohanty, and C. Peterson. Folding lattice proteins with quantum annealing. *Physical Review Research*, 4(4):043013, 2022. [arXiv:2205.06084](#).
- [60] B. Isralewitz, M. Gao, and K. Schulten. Steered molecular dynamics and mechanical functions of proteins. *Current opinion in structural biology*, 11(2):224–230, 2001.
- [61] S. Izrailev, S. Stepaniants, B. Isralewitz, D. Kosztin, H. Lu, F. Molnar, W. Wriggers, and K. Schulten. Steered molecular dynamics. In *Computational Molecular Dynamics: Challenges, Methods, Ideas: Proceedings of the 2nd International Symposium on Algorithms for Macromolecular Modelling, Berlin, May 21–24, 1997*, pages 39–65. Springer, 1999.
- [62] S. Jaques and A. G. Rattew. QRAM: A survey and critique, 2023. [arXiv:2305.10310](#).
- [63] J. Jumper, R. Evans, A. Pritzel, T. Green, M. Figurnov, O. Ronneberger, K. Tunyasuvunakool, R. Bates, A. Žídek, A. Potapenko, et al. Highly accurate protein structure prediction with alphafold. *Nature*, 596(7873):583–589, 2021.
- [64] C. Kamp and K. Christensen. Spectral analysis of protein-protein interactions in drosophila melanogaster. *Physical Review E*, 71(4):041911, 2005. [arXiv:q-bio/0405021](#).
- [65] K. S. Keating, S. C. Flores, M. B. Gerstein, and L. A. Kuhn. Stonehinge: hinge prediction by network analysis of individual protein structures. *Protein Science*, 18(2):359–371, 2009.
- [66] I. Kerenidis and A. Prakash. Quantum recommendation systems, 2016. [arXiv:1603.08675](#).
- [67] D. E. Kirk. *Optimal control theory: an introduction*. Courier Corporation, 2004.
- [68] J. L. Klepeis, K. Lindorff-Larsen, R. O. Dror, and D. E. Shaw. Long-timescale molecular dynamics simulations of protein structure and function. *Current opinion in structural biology*, 19(2):120–127, 2009.
- [69] M. Kliesch, T. Barthel, C. Gogolin, M. J. Kastoryano, and J. Eisert. Dissipative quantum Church-Turing theorem. *Physical Review Letters*, 107(12), 2011. [arXiv:1105.3986](#).
- [70] A. R. Leach. *Molecular modelling: principles and applications*. Pearson education, 2001.
- [71] G. Li and Q. Cui. A coarse-grained normal mode approach for macromolecules: an efficient implementation and application to Ca<sup>2+</sup>-ATPase. *Biophysical Journal*, 83(5):2457–2474, 2002.
- [72] H. Li, H. Ni, and L. Ying. On low-depth quantum algorithms for robust multiple-phase estimation, 2023. [arXiv:2303.08099](#).

- [73] X. Li and C. Wang. Efficient quantum algorithms for quantum optimal control. In *International Conference on Machine Learning*, pages 19982–19994. PMLR, 2023. [arXiv:2304.02613](#).
- [74] X. Li and C. Wang. Succinct description and efficient simulation of non-Markovian open quantum systems. *Communications in Mathematical Physics*, 401(1):147–183, 2023. [arXiv:2111.03240](#).
- [75] A. N. Lima, R. J. de Oliveira, A. S. K. Braz, M. G. de Souza Costa, D. Perahia, and L. P. B. Scott. Effects of ph and aggregation in the human prion conversion into scrapie form: a study using molecular dynamics with excited normal modes. *European Biophysics Journal*, 47:583–590, 2018.
- [76] L. Lin and Y. Tong. Near-optimal ground state preparation. *Quantum*, 4:372, 2020. [arXiv:2002.12508](#).
- [77] L. Lin and Y. Tong. Optimal quantum eigenstate filtering with application to solving quantum linear systems. *Quantum*, 4:361, 2020. [arXiv:1910.14596](#).
- [78] L. Lin and Y. Tong. Heisenberg-limited ground-state energy estimation for early fault-tolerant quantum computers. *PRX Quantum*, 3(1):010318, 2022. [arXiv:2102.11340](#).
- [79] K. Lindorff-Larsen, S. Piana, R. O. Dror, and D. E. Shaw. How fast-folding proteins fold. *Science*, 334(6055):517–520, 2011.
- [80] H. Linn, I. Brundin, L. García-Álvarez, and G. Johansson. Resource analysis of quantum algorithms for coarse-grained protein folding models, 2023. [arXiv:2311.04186](#).
- [81] J.-P. Liu, D. An, D. Fang, J. Wang, G. H. Low, and S. Jordan. Efficient quantum algorithm for nonlinear reaction–diffusion equations and energy estimation. *Communications in Mathematical Physics*, 404(2):963–1020, 2023. [arXiv:2205.01141](#).
- [82] J.-P. Liu, H. Ø. Kolden, H. K. Krovi, N. F. Loureiro, K. Trivisa, and A. M. Childs. Efficient quantum algorithm for dissipative nonlinear differential equations. *Proceedings of the National Academy of Sciences*, 118(35):e2026805118, 2021. [arXiv:2011.03185](#).
- [83] J.-P. Liu and L. Lin. Dense outputs from quantum simulations. *Journal of Computational Physics*, 514:113213, 2024. [arXiv:2307.14441](#).
- [84] S. Lloyd. Universal quantum simulators. *Science*, pages 1073–1078, 1996.
- [85] G. H. Low and I. L. Chuang. Optimal Hamiltonian simulation by quantum signal processing. *Physical Review Letters*, 118(1):010501, 2017. [arXiv:1606.02685](#).
- [86] G. H. Low and I. L. Chuang. Hamiltonian simulation by qubitization. *Quantum*, 3:163, 2019. [arXiv:1610.06546](#).

- [87] A. D. MacKerell Jr, D. Bashford, M. Bellott, R. L. Dunbrack Jr, J. D. Evanseck, M. J. Field, S. Fischer, J. Gao, H. Guo, S. Ha, et al. All-atom empirical potential for molecular modeling and dynamics studies of proteins. *The journal of physical chemistry B*, 102(18):3586–3616, 1998.
- [88] H. Ni, H. Li, and L. Ying. On low-depth algorithms for quantum phase estimation. *Quantum*, 7:1165, 2023. [arXiv:2302.02454](#).
- [89] K. Phalak, M. Alam, A. Ash-Saki, R. O. Topaloglu, and S. Ghosh. Optimization of quantum read-only memory circuits, 2022. [arXiv:2204.03097](#).
- [90] M. Pocrnic, D. Segal, and N. Wiebe. Quantum simulation of Lindbladian dynamics via repeated interactions. 2023. [arXiv:2312.05371](#).
- [91] J. A. Rackers, Z. Wang, C. Lu, M. L. Laury, L. Lagardère, M. J. Schnieders, J.-P. Piquemal, P. Ren, and J. W. Ponder. Tinker 8: software tools for molecular design. *Journal of chemical theory and computation*, 14(10):5273–5289, 2018.
- [92] P. Rall. Quantum algorithms for estimating physical quantities using block encodings. *Physical Review A*, 102(2):022408, 2020. [arXiv:2004.06832](#).
- [93] A. Robert, P. K. Barkoutsos, S. Woerner, and I. Tavernelli. Resource-efficient quantum algorithm for protein folding. *npj Quantum Information*, 7(1):38, 2021. [arXiv:1908.02163](#).
- [94] J. K. Salmon, M. A. Moraes, R. O. Dror, and D. E. Shaw. Parallel random numbers: as easy as 1, 2, 3. In *Proceedings of 2011 international conference for high performance computing, networking, storage and analysis*, pages 1–12, 2011.
- [95] T. Schlick. *Molecular modeling and simulation: an interdisciplinary guide*, volume 2. Springer, 2010.
- [96] S. Subramanian and M.-H. Hsieh. Quantum algorithm for estimating  $\alpha$ -renyi entropies of quantum states. *Physical Review A*, 104(2):022428, 2021. [arXiv:1804.01973](#).
- [97] S. Takahira, A. Ohashi, T. Sogabe, and T. S. Usuda. Quantum algorithms based on the block-encoding framework for matrix functions by contour integrals, 2021. [arXiv:2106.08076](#).
- [98] F. Tama, F. X. Gadea, O. Marques, and Y.-H. Sanejouand. Building-block approach for determining low-frequency normal modes of macromolecules. *Proteins: Structure, Function, and Bioinformatics*, 41(1):1–7, 2000.
- [99] Y. Tong, D. An, N. Wiebe, and L. Lin. Fast inversion, preconditioned quantum linear system solvers, fast Green’s-function computation, and fast evaluation of matrix functions. *Physical Review A*, 104(3):032422, 2021. [arXiv:2008.13295](#).

- [100] C. Wang and L. Wossnig. A quantum algorithm for simulating non-sparse Hamiltonians, 2018. [arXiv:1803.08273](#).
- [101] B. Widynski. Squares: a fast counter-based rng, 2020. [arXiv:2004.06278](#).
- [102] K. M. Yip, N. Fischer, E. Paknia, A. Chari, and H. Stark. Atomic-resolution protein structure determination by cryo-em. *Nature*, 587(7832):157–161, 2020.

## A Some overview of specific NMA models

Here we give an overview of some of the existing models. All these models can be recast into linear differential equations in (3.2), while the matrix  $K$  can be modeled differently. Overall, the underlying assumption in NMA is that any given equilibrium system fluctuates about a single well-defined conformation and that the nature of these thermally induced fluctuations can be calculated assuming a simple harmonic form for the potential. In NMA, a protein consists of a collection of nodes, here labeled by  $i \in [N] := \{1, 2, \dots, N\}$ . Further, we denote the instantaneous position of the  $i$ -th node by  $R_i$  with equilibrium position  $R_i^0$ . Therefore the dynamics is reflected in the displacement vector  $\mathbf{u}_i = R_i - R_i^0$ . We also denote the relative position between two atoms,  $i$  and  $j$ , by  $\mathbf{u}_{ij} = R_i - R_j$  with equilibrium values  $R_{ij}^0$ .

An intuitive interpretation of the NMA model is that every pair of neighboring nodes is connected by a spring with a spring constant given by  $K_{i,j}$ . Therefore the total potential energy is given by the following quadratic form,

$$V(\mathbf{u}) = \frac{1}{2} \sum_{ij=1}^N \mathbf{u}_i K_{ij} \mathbf{u}_j. \quad (\text{A.1})$$

Then the equations in (3.2) follow directly from standard Hamilton or least-action principle.

A solution of (3.2) has the form  $\hat{\mathbf{u}}_k(t) = \mathbf{a}_k \exp(-i\omega_k t)$ , where  $a_k$  contains both the amplitude and phase factor, and  $\omega_k$  is the frequency. The equation of motion becomes

$$\omega_k^2 M \hat{\mathbf{u}}_k = K \hat{\mathbf{u}}_k, \quad (\text{A.2})$$

or a matrix diagonalization form,

$$KU = MU\Lambda, \quad (\text{A.3})$$

where  $U$  collects  $\{K\hat{\mathbf{u}}_k\}_k$  as its columns and  $\Lambda$  collects  $\{\omega_k^2\}_k$  as its diagonal elements.

In the energy spectrum,  $\omega_k$  corresponds to the vibration frequency and the associated normal mode  $\hat{\mathbf{u}}_k$  carries energy,

$$V(\mathbf{u}) = \frac{1}{2} \hat{\mathbf{u}}_k^T K \hat{\mathbf{u}}_k = \frac{\omega_k^2}{2}. \quad (\text{A.4})$$

The vibration frequencies are usually divided into low (or soft) modes, which indicate a less steep gradient along the energy landscape and thus energetically favorable, and high-frequency (or excited) modes, which require much higher thermal energy to reach. Displacements along high-frequency modes are therefore energetically more expensive than those of equal magnitude along

low-frequency modes. The vibrational energy is, on average, equally partitioned among all the modes, such that the average amplitude of oscillation along mode  $k$  scales with  $1/\omega_k^2$ . Thus, the molecule experiences the greatest displacement along the lowest frequency, or “slowest”, modes. Conceptually, the energy landscape slopes most gently along the slow modes, and these are consequently the most accessible. These modes are also of great interest when seeking to determine the most probable global fluctuations of a molecule. Large eigenvalues, on the other hand, indicate directions of steep energetic ascent, and excursions along these modes will quickly raise the system’s energy.

In the following sections, we will give several examples of the stiffness matrix  $K$  as well as the matrix structure, which will be important in the preparation of the quantum algorithms. Further generalizations, including the interactions with the solvent and the presence of external forces, will be presented later in Sections 3.2 and 3.3.

### A.1 Normal Modes of All-atom Models

A normal mode model can be directly obtained from MD (3.2) by a Taylor expansion. Specifically, at an equilibrium configuration  $\{R_i^0, i \in [N]\}$ , the force on each atom vanishes, i.e.,  $\nabla V(R_1^0, R_2^0, \dots, R_N^0) = 0$ . Thus a Taylor expansion up to second-order yields,

$$V(R_1, R_2, \dots, R_N) \approx V(R_1^0, R_2^0, \dots, R_N^0) + \frac{1}{2} \sum_{i,j=1}^N \mathbf{u}_i^T K_{i,j} \mathbf{u}_j, \quad (\text{A.5})$$

where  $\mathbf{u}_i := R_i - R_i^0$  indicates the displacement from the equilibrium position. In addition,

$$K_{i,j} := \nabla_{R_i, R_j}^2 V(R_1^0, R_2^0, \dots, R_N^0), \quad (\text{A.6})$$

corresponds to the  $(i, j)$  block of the Hessian matrix, and it is often referred to as the force constant matrix. The translational symmetry implies that [9],

$$\sum_{j=1}^N K_{i,j} = 0. \quad (\text{A.7})$$

Meanwhile, the approximation (A.5) is known as a harmonic approximation, which simplifies the equations of motion to a linear ODE system in (3.2). In other words, the elements of the stiffness matrix  $K$  are obtained from the hessian of the interatomic potential  $V$  at an equilibrium.

### A.2 Network models

Another widely used model for normal mode calculations is based on mapping protein structures to a network, where the connectivity is represented by the edges of the network. It has been motivated by the observation that the low modes typically correspond to the cooperative movement of the  $C^\alpha$  atoms on the backbone [15], which can be qualitatively described by an elastic network. This idea has been later generalized to incorporate anisotropic motions and networks of all the

atoms. Typically, in a network model, one designates a set of nodes that correspond to either the displacement of the  $C^\alpha$  atoms or all the atoms in the molecule, with displacement denoted by  $\mathbf{u} \in \mathbb{R}^M$ . The vibration potential is then expressed as,

$$V = \frac{1}{2} \mathbf{u}^T \Gamma \mathbf{u}. \quad (\text{A.8})$$

The matrix  $\Gamma$  is a symmetric semi-positive definite matrix known as the Kirchhoff or connectivity matrix. The elements in  $\Gamma$  can be interpreted as the weights in the network. They are designated empirically, rather than computed from the force field, which drastically simplifies the accessibility of the models. Thus, the variation among different network models comes from the designations of the nodes  $\Delta R$  and the specifications of the Kirchhoff matrix.

### A.2.1 Gaussian network model

The Gaussian network model [14, 54] works directly with the  $C^\alpha$  atoms and is built on the assumption that the relative distance between  $C^\alpha$  atoms follows a Gaussian distribution. The coupling of the  $C^\alpha$  atoms is modelled by a connectivity matrix  $\Gamma$ , with elements  $\Gamma_{ij}$  selected as the Laplacian matrix of inter-residue contacts,

$$\Gamma_{ij} = \begin{cases} -1, & i \neq j, R_{ij}^0 \leq r_c, \\ 0, & i \neq j, R_{ij}^0 > r_c, \\ -\sum_{j, j \neq i} \Gamma_{ij}, & i = j. \end{cases} \quad (\text{A.9})$$

The parameter  $r_c$  is a cut-off radius that identifies neighboring  $C^\alpha$  atoms. Meanwhile, the stiffness matrix  $K$  is set to  $K = \gamma \Gamma$  with  $\gamma$  being a force constant uniform for all connected nodes.

### A.2.2 Anisotropic network model

Implicit in the GNM model is that the displacement of each node is isotropic, in that the components  $\Delta X$ ,  $\Delta Y$ , and  $\Delta Z$  are independent and identically distributed, given by the distribution of  $\Delta R$ . The Anisotropic Network Model (ANM) [10] is an extension of GNM to include all three coordinates for each  $C^\alpha$  atom, thus accounting for directional movements. In this case, we can write  $R_i = [X_i, Y_i, Z_i]$ ,  $R_j = [X_j, Y_j, Z_j]$  be the instantaneous positions of atoms  $i$  and  $j$ . Further, let  $R_{ij} = R_i - R_j$  be the relative position, with  $d_{ij}$  be the equilibrium distance. In ANM, the Kirchhoff matrix is obtained by assuming that the energy between the two atoms is modeled by a harmonic spring with spring constant  $\gamma$ ,

$$V_{ij} = \frac{\gamma}{2} (\|R_{ij}\| - d_{ij})^2. \quad (\text{A.10})$$

Therefore, by taking the second-order derivatives, one has,

$$\frac{\partial^2 V_{ij}}{\partial X_i^2} = \frac{\partial^2 V_{ij}}{\partial X_j^2} = \frac{\gamma}{d_{ij}^2} (X_j - X_i)^2, \quad \frac{\partial^2 V_{ij}}{\partial X_i \partial Y_j} = -\frac{\gamma}{d_{ij}^2} (X_j - X_i)(Y_j - Y_i). \quad (\text{A.11})$$

As a result, the matrix  $K$  can be expressed in a block form,  $[K_{i,j}]$  with each block being a  $3 \times 3$  matrix,

$$K_{ij} = \begin{cases} -\frac{\gamma}{d_{ij}^2} R_{ij}^0 (R_{ij}^0)^T, & i \neq j \\ -\sum_{j \neq i} K_{ij}, & i = j. \end{cases} \quad (\text{A.12})$$

### A.2.3 Network Models with Distance-Dependent Force Constants

In GNM and ANM, the elastic springs are introduced between atoms within a certain proximity, i.e., when the distance is within a cut-off radius. This can be accomplished by choosing  $K_{ij} = 0$ , where the distance between the two atoms  $d_{ij} > r_c$ . Fuglebakk [49] extended this choice by introducing a distance dependence in  $K$ . For example, in the Harmonic  $C^\alpha$  Potential Model (HCA), the force constants are given by

$$K_{ij} = \begin{cases} a_1 d_{ij} - b, & i \neq j, d_{ij} \leq r_c \\ a_2 d_{ij}^{-6}, & i \neq j, d_{ij} > r_c. \end{cases} \quad (\text{A.13})$$

Here the parameter  $r_c$  is set to be 0.4 nm to separate interactions between  $C_\alpha$  atoms adjacent in sequence from the other interactions. Long-range interactions are proportional to an inverse power of six of the equilibrium distance between the interacting modes. The parameters  $a_1$ ,  $a_2$ ,  $b$  are chosen by fitting an all-atom normal mode calculation for crambin.

Another important approach is the parameter-free anisotropic network model (pfANM), which defines force constants by the inverse-square of the equilibrium distance between the interacting modes. A similar example is the Realistic Extension Algorithm via Covariance Hessian (REACH), which offers a refined treatment for the force constants to incorporate the backbone interactions.

### A.2.4 All-atom normal mode analysis

As illustrated in Appendix A.1, the normal mode analysis can be derived from the full atomistic description with  $K$  corresponding to the hessian of the potential energy. In practice, however, this can be quite a cumbersome effort. Hu et al [57] proposed to consider atoms as point masses and model the bonding between atoms as elastic springs, thus empirically mapping the atomistic model to an elastic network. The total elastic energy is also a quadratic form Eq. (A.8) and the stiffness parameters in [57] are chosen based on the interatomic distance,

$$K_{ij} = \begin{cases} C_{\text{nonbonded}}, & d_{ij} \leq l_1 \\ C_{\text{nonbonded}} \cdot \exp\{-(d_{ij} - l_1)\}, & l_1 \leq d_{ij} \leq l_2 \\ 0, & d_{ij} \geq l_2. \end{cases} \quad (\text{A.14})$$

Here  $d_{ij}$  is the distance between two atoms:  $d_{ij} = \|R_i^0 - R_j^0\|$ ,  $C_{\text{bonded}} = 7 \times 10^5$  dyne/cm is a nominal spring constant generally assigned to a single bond, and  $C_{\text{nonbonded}} = 6 \times 10^3$  dyne/cm is for non-bonded interactions,  $l_1$  and  $l_2$  are the lower and upper cutoff values, under the consideration of the maximum range of van der Waals interaction, e.g.,  $l_1 = 2\text{\AA}$ , and upper-bound cutoff distance



$l_2 = 8\text{\AA}$ . This model is later extended [58], where the stiffness matrix ( $k_{i,j}$ ) is determined based on the chemical connectivity and atomic interaction, rather than the cutoff-distance.

## B Hierarchical coarse-graining

Coarse-grained models are commonly employed to describe the structure and dynamics of large molecular systems.

We build a hierarchical network model based on Markov stochastics [44, 28, 29]: step (i) map the structure to its optimal reduced level representation. This step may involve several intermediate levels of resolution; step (ii) performs structural analysis (e.g. ENM, GNM) at a coarse-grained scale; and step (iii) reconstructs the detailed structure-dynamics. The communication/coupling of residues at a given level is assumed to obey a Markov process controlled by atom-atom contact topology. The steps (i) and (iii) are achieved by two operators,  $R$  for model reduction, and  $K$  for model reconstruction.  $R$  and  $K$  ensure that similar stochastic characteristics are retained between successive levels of the hierarchy.

We model each protein as a weighted, undirected graph  $G = (V, E)$ , with residues  $V = \{v_1, \dots, v_n\}$  and interactions  $E = \{e_{ij}\}$ . The set of all pairwise interactions is described by a non-negative, symmetric affinity matrix  $A$ , with element  $a_{ij} = a_{ji}$ . The element  $a_{ij} = N_{ij}$  is the total number of atom-atom contacts made between residues  $v_i, v_j$  and within a cutoff distance  $r_c = 4.5\text{\AA}$ . The self-similar contact  $a_{ii}$  is similarly defined, but all bonded pairs are excluded. An alternative definition is  $a_{ij} = N_{ij}/\sqrt{N_i N_j}$ , where  $N_i$  is the total number of atoms in the residue  $v_i$ .

This representation takes into account the difference in the size of amino acids, and captures to a first approximation the strong (weak) interactions expected to arise between residue pairs with a large (small) number of atom-atom contacts.

The degree of the residue  $v_i$  is defined as  $d_i = \sum_{j=1}^n a_{ij}$ . We define  $D = \text{diag}(d_1, \dots, d_n)$ .

We define a Markov transition matrix on the protein graph as  $M = AD^{-1}$ , with element  $m_{ij} = a_{ij}d_i^{-1}$  as the probability of transition from residue  $v_i$  to  $v_j$ . The Markov chain has a unique stationary distribution  $\pi$  with  $\pi_i = d_i/(\sum_{j=1}^n d_j)$ .

The objective in designing a network hierarchy is to map the Markov process operating at the highest resolution onto successively lower resolution network models, while maintaining its stochastic characteristics. Using the  $n \times n$  Markov transition matrix  $M$  and stationary distribution  $\pi$ , we build a  $m \times m$  coarse-scale Markov transition matrix  $\widetilde{M}$  ( $m \ll n$ ) and its stationary distribution  $\delta$ . To build a hierarchy of intermediate resolution networks, we devise two operators at each level of the hierarchy:  $R$  for model reduction, and  $K$  for model reconstruction.

We express  $\pi$  as a mixture of latent distributions

$$\pi = K\delta, \tag{B.1}$$

where  $\delta$  is a unknown stationary distribution in the reduced space and  $K = \{K_{ij}\}$  is an  $n \times m$  non-negative kernel matrix, acting as an expansion operator.

We derive a maximum likelihood approximation for  $\delta$  using an Expectation-Maximization (EM) algorithm. We minimize the Kullback-Liebler divergence subject to the constraint  $\sum_{j=1}^m \delta_j = 1$  ensured by the Lagrange multiplier  $\lambda$

$$E = - \sum_{i=1}^n \pi_i \ln \sum_{j=1}^m K_{ij} \delta_j + \lambda (\sum_{j=1}^m \delta_j - 1). \quad (\text{B.2})$$

Taking the derivative of  $E$  with respect to  $\delta_j$  to be zero, we obtain

$$\sum_{i=1}^n \frac{\pi_i K_{ij} \delta_j}{\sum_{k=1}^m K_{ik} \delta_k} = \lambda \delta_j. \quad (\text{B.3})$$

We can define ownership of the node  $i$  in the high resolution to the kernel  $j$  in the low resolution as

$$R_{ij} = \frac{K_{ij} \delta_j}{\sum_{k=1}^m K_{ik} \delta_k} \quad (\text{B.4})$$

with  $\sum_{j=1}^m R_{ij} = 1$ . Using the relation and  $\sum_{j=1}^m \delta_j = 1$  and  $\sum_{i=1}^n \pi_i = 1$ , it gives  $\lambda = 1$ . This leads to the stationary distribution  $\delta$  at the coarse scale

$$\delta_j = \sum_{i=1}^n \pi_i R_{ij}. \quad (\text{B.5})$$

$R = \{R_{ij}\}$  maps  $\pi$  to  $\delta$ , acting as a reduction operator. Following Bayes theorem,

$$K_{ij} = \frac{R_{ij} \pi_i}{\delta_j}. \quad (\text{B.6})$$

The operations  $K$  and  $R$  and stationary distribution  $\delta$  can be computed using the EM-type procedure: (i) select an initial estimate for  $K$  and  $\delta$ ; (ii) E-step: compute ownership map  $R$  using  $R_{ij} = \frac{K_{ij} \delta_j}{\sum_{k=1}^m K_{ik} \delta_k}$ ; (iii) M-step: compute  $K$  and  $\delta$  using  $\delta_j = \sum_{i=1}^n \pi_i R_{ij}$  and  $K_{ij} = \frac{R_{ij} \pi_i}{\delta_j}$ ; repeat E- and M-steps until convergence.

The Markov transition matrix in the coarse-grained representation  $\widetilde{M}$  follows

$$\widetilde{M} = \text{diag}(\delta) K^\top \text{diag}(K \delta)^{-1} K. \quad (\text{B.7})$$

We can generate a symmetric affinity matrix  $\widetilde{A}$  that describes the interactions in the low-resolution network

$$\widetilde{A} = \widetilde{M} \text{diag}(\delta). \quad (\text{B.8})$$

## C QROM based on direct quantization of classical ROM

There exist several polylog( $N$ )-depth implementations of QROM [66] with the cost of  $O(N)$  qubits involved. Here, we introduce a direct quantization of the classical ROM which features polylog( $N$ ) depth, and supports arbitrary trade-offs between circuit depth and qubit number.

### C.1 1-of- $N$ decoder

A classical ROM contains 2 parts. Part 1 is a binary decoder, or more precisely a 1-of- $N$  decoder, which translates the binary address to a 1-of- $N$  representation. For instance, if the input address is  $5 = |101\rangle$ , then the output should be  $|0000100\dots\rangle$  where only the 5th qubit has value 1. Quantum binary decoder can be implemented by a polylog( $N$ )-depth circuit with  $O(N)$  qubits. The gate implementation is shown below where we start by considering a 1-of-2 decoder.

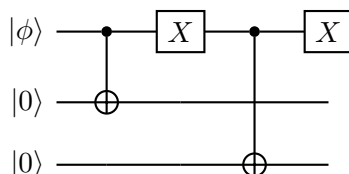


Figure 6: The 1-of-2 decoer.

Any 1-to- $2^n$  decoder can be constructed by applying 1-of- $(2^{n-1})$  twice. For example, the 1-of-4 decoder can be made by 2 1-of-2 decoders.

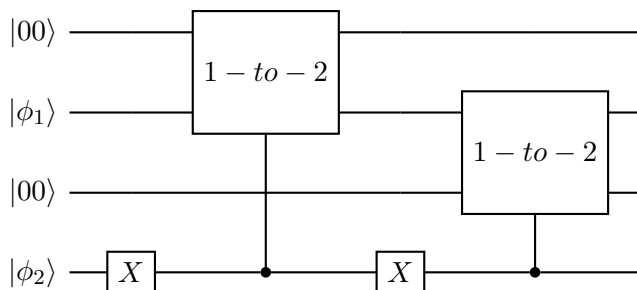


Figure 7: The 2-to-4 decoder.

### C.2 Hard-coded data loader

Once the binary number is decoded as the 1-of- $N$  representation, the data can be loaded by  $m$  layers of large OR-type CNOT gates which performs the  $X$  gate if *any* of the control qubits is 1, where  $m$  is the length of the data of each element. In this paper,  $m$  represents the precision of initial positions of the atoms or residues.

The large OR-type CNOT gate can be implemented by  $O(\log N)$  layers of OR gates and a single CNOT gate, thus is also depth-efficient.

### C.3 State-based data loader

A more flexible method is to store the classical data in some data states that can be called, instead of hard-coding them as the gates, and apply CCNOT gates to copy them into the output qubits, as shown in Figure 9. Note that the CCNOT gates here are the normal CCNOT: if both control

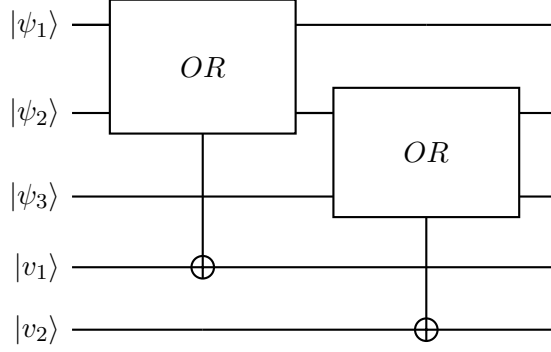


Figure 8: The data loader for the following dictionary:  $\{1 \rightarrow 10, 2 \rightarrow 11, 3 \rightarrow 01\}$

qubits are in  $|1\rangle$ , then the  $X$  gate is applied to the target qubit, unlike in the hard-coded data loader.

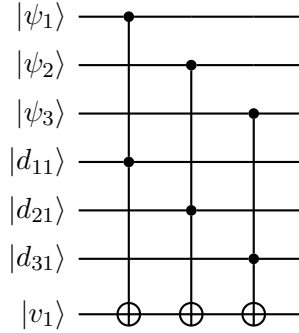


Figure 9: The state-based data loader for a dictionary of 3 indices with single-qubit data.

Similar techniques can be used to reduce its depth to  $O(\log N \log M)$ .  $N$  CCNOT gates acting on the same target qubit can be considered as a large OR-CCNOT gate (the Pauli operator  $X_j$  on the  $j$ th output qubit is applied if any pair of  $|\psi_i\rangle$  and  $|d_{ij}\rangle$ ) is in  $|1\rangle|1\rangle$ , which can be implemented by one layer of parallel AND gates and  $O(\log N)$  layers of OR gates.

The construction described above has  $\text{polylog}N$ -depth and  $O(N)$ -width. However, on a specific platform implementing the algorithm, a narrower but deeper circuit might be preferred to increase its performance. Our QROM implementation based on hard-coded loader features a trade-off between qubit number and circuit depth, as shown in the following theorem.

**Theorem C.1** (Width-depth trade-off of QROM). *For arbitrary  $k \in \{0, 1, \dots, n\}$ , there is a hard-coded QROM implementation with  $O(2^{n-k})$  qubits and  $O(2^k m \cdot \text{poly}(n))$  circuit depth, where  $2^n$  is the number of indices, and  $m$  is the number of bits of each data  $v_i$  corresponding to the  $i$ th index.*

*Proof.* For  $k = 0$ , this is the original hard-coded version QROM, where  $n$  bits of the input index is translated to the 1-of- $2^n$  format using a  $\text{poly}(n)$ -depth decoder and the data is loaded using  $O(m)$  layers of  $\text{poly}(n)$ -depth OR-type CNOT gates. The total number of qubits is  $O(2^n)$ .

To reduce the qubit number by half, one can choose not to decode the most significant bit (MSB) in the 1-of- $N$  decoder, and run 2 different data loader circuits conditioned on different values of the MSB to load the information corresponding to MSB=0 and MSB=1, respectively, as shown in Figure 10. Such a reduction can be run for arbitrarily many significant bits, and for every bit the qubit number is halved while the circuit depth is doubled. Therefore, for any  $k \in \{0, 1, \dots, n\}$  the qubit number can be reduced to  $O(2^{n-k})$ , and the circuit depth becomes  $O(2^k m \cdot \text{poly}(n))$  for  $k$  times of trade-off.  $\square$

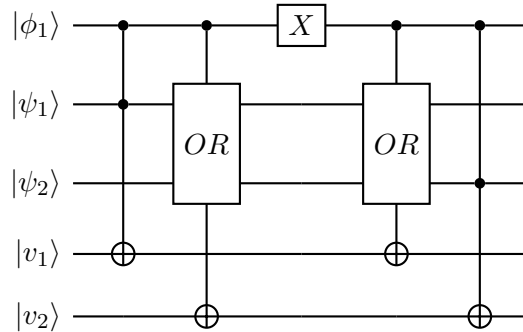


Figure 10: The data loader with a  $k = 1$  depth-width trade-off for the following dictionary:  $\{1 \rightarrow 10, 2 \rightarrow 11, 3 \rightarrow 11, 4 \rightarrow 01\}$